Am J Transl Res 2026;18(5):3942-3960
www.ajtr.org /ISSN:1943-8141/AJTR0171900

Original Article

KDM4D enhances radiosensitivity in esophageal squamous cell carcinoma through the SRBD1/RPL11/c-Myc/WIP1/CHK1 axis

Zhenhua Gao[1], Xiaoyun Han[2], Shuanghu Yuan[1,3]

[1]*Department of Radiation Oncology, Shandong University Cancer Center, Jinan 250012, Shandong, China;*
[2]*Department of Gynecological Oncology, Shandong University Cancer Center, Jinan 250012, Shandong, China;*
[3]*Department of Radiation Oncology, The First Affiliated Hospital of USTC, Division of Life Sciences and Medicine, University of Science and Technology of China, Hefei 230001, Anhui, China*

Received February 5, 2026; Accepted April 20, 2026; Epub May 15, 2026; Published May 30, 2026

Abstract: *Background:* Radioresistance is a critical challenge in the treatment of esophageal squamous cell carcinoma (ESCC). Histone lysine-specific demethylase 4D (KDM4D) has been implicated in DNA damage response; however, its role in regulating ESCC radiosensitivity remained unclear. We hypothesized KDM4D modulates radiosensitivity through the c-Myc/checkpoint kinase 1 (CHK1) pathway. *Objective:* To investigate the role of KDM4D in ESCC radiosensitivity and to elucidate the underlying molecular mechanisms. *Methods:* KDM4D expression was analyzed in tumor samples from 32 ESCC patients who received neoadjuvant radiotherapy. ESCC cell lines with KDM4D knockdown or overexpression were subjected to irradiation, and radiosensitivity was evaluated. Chromatin immunoprecipitation-polymerase chain reaction (ChIP-PCR), luciferase assay, and xenograft models were used to explore the underlying mechanisms. *Results:* Elevated KDM4D expression was associated with improved response to radiotherapy and prolonged progression-free survival (PFS). KDM4D knockdown significantly reduced radiation-induced apoptosis. Mechanistically, KDM4D promoted the demethylation of histone H3 lysine 9 trimethylation (H3K9me3), thereby activating S1 RNA-binding domain-containing protein 1 (SRBD1). SRBD1 subsequently upregulated ribosomal protein L11 (RPL11), which suppressed c-Myc expression, thereby downregulating wild-type p53-induced phosphatase 1 (WIP1) and CHK1. Rescue experiments and xenograft studies further verified this regulatory axis. *Conclusion:* KDM4D enhances ESCC radiosensitivity through the SRBD1/RPL11/c-Myc/WIP1/CHK1 pathway, highlighting its potential as both a diagnostic biomarker and a therapeutic target.

Keywords: Esophageal squamous cell carcinoma, radiosensitivity, KDM4D, SRBD1, RPL11, c-Myc, CHK1, WIP1, histone demethylation, neoadjuvant radiotherapy

Introduction

Esophageal squamous cell carcinoma (ESCC), a highly aggressive malignancy, exhibits an extraordinarily high incidence rate in East Asia [1]. Despite advances in multimodal therapy, the overall survival of ESCC patients remains poor, primarily due to local recurrence and distant metastasis [2]. Neoadjuvant chemoradiotherapy has emerged as the standard treatment for locally advanced ESCC, providing improved locoregional control and potential downstaging benefits [3]. However, a substantial proportion of patients display resistance to radiotherapy, leading to treatment failure and unfavorable outcomes [4].

Radioresistance in tumor cells is a complex biological process driven by diverse factors, such as improved DNA damage repair efficiency, dysregulated cell cycle checkpoint activation, and increased anti-apoptotic signaling [5]. Among the key regulators of radioresistance, the proto-oncogene c-Myc plays a central role by transcriptionally activating checkpoint kinases CHK1 and CHK2, thereby facilitating DNA damage repair and cell cycle arrest [6]. The phosphatase WIP1 (PPM1D) further contributes to radioresistance by dephosphorylating CHK1 at Ser345 and p53 at Ser15, thereby attenuating checkpoint signaling and promoting cell cycle re-entry following DNA damage [7]. Therefore, elucidating the upstream regulatory mecha-

https://doi.org/10.62347/GWRN1389

nisms of the c-Myc/WIP1/CHK1 axis may provide novel therapeutic strategies to enhance radiosensitivity in ESCC.

Among epigenetic alterations, histone methylation plays a pivotal role in governing gene transcription, chromatin organization, and cellular adaptive responses to genotoxic stress [8]. The lysine-specific demethylase 4 (KDM4) family, which comprises KDM4A-D, catalyzes the removal of di- and tri-methylation marks from H3K9 and H3K36, thereby modulating transcription and DNA damage repair [9]. Among these family members, KDM4D (also referred to as JMJD2D) is structurally distinct from KDM4A-C, as it lacks the plant homeodomain (PHD) and Tudor domains, and has been implicated in the DNA damage response through PARP1-dependent recruitment to double-strand break sites [10]. Evidence indicates that KDM4 family members are involved in regulating radioresistance across various cancers [11, 12]. Nevertheless, the role of KDM4D in modulating ESCC radiosensitivity and the underlying molecular mechanisms remain to be investigated systematically.

Ribosomal protein L11 (RPL11) has been identified as a critical tumor suppressor that negatively regulates c-Myc activity through both direct protein-protein interaction that blocks c-Myc-dependent transcription and facilitation of c-Myc mRNA degradation through the RNA-induced silencing complex (RISC) pathway [13, 14]. S1 RNA-binding domain-containing protein 1 (SRBD1) has been associated with glaucoma and apoptosis regulation; however, its role in cancer and its relationship with the RPL11/c-Myc axis remain poorly defined [15]. Recent evidence suggests that SRBD1 regulates RPL11 expression and mediates tumor suppression by the RPL11-MDM2-p53 pathway [16], raising the possibility that SRBD1 may serve as a link between epigenetic regulation and RPL11/c-Myc signaling.

In this study, we investigated the role of KDM4D in modulating the radiosensitivity of ESCC and further illuminated the underlying molecular mechanisms. We found that KDM4D expression is positively associated with a favorable response to neoadjuvant radiotherapy in ESCC patients. Mechanistically, KDM4D activates SRBD1 transcription by mediating H3K9me3 demethylation at intron 1 of the SRBD1 gene, which subsequently upregulates RPL11 expression. Elevated RPL11 suppresses c-Myc activity, leading to the downregulation of WIP1 and CHK1, sustained p-CHK1 activation, and enhanced radiation-induced apoptosis. Our findings identify a novel KDM4D-SRBD1-RPL11-c-Myc-WIP1-CHK1 signaling axis that regulates radiosensitivity in ESCC, providing potential biomarkers for predicting radiotherapy response and therapeutic targets for radiosensitization.

Materials and methods

Clinical samples and ethics statement

A total of 32 ESCC tissue samples were collected from patients who underwent neoadjuvant chemoradiotherapy followed by surgical resection at Shandong Cancer Hospital (Jinan, China). All patients received standard neoadjuvant chemoradiotherapy, consisting of 40-50 Gy of radiation delivered in 20-25 fractions combined with platinum-based chemotherapy. Tumor response was evaluated according to the tumor regression grade (TRG) system. TRG 0-1 was defined as a favorable response, indicating complete or near-complete tumor regression, whereas TRG 2-3 was defined as a non-response, representing partial or minimal regression. Among the 32 patients, 11 achieved a favorable response (TRG 0-1) and 21 were categorized as non-response (TRG 2-3). For prognostic analysis, patients were stratified into high (n = 9) and low (n = 23) KDM4D expression groups, and progression-free survival (PFS) was assessed. Written informed consent was obtained from all participants prior to specimen collection.

All animal experiments were approved by the Institutional Animal Care and Use Committee of The First Affiliated Hospital of USTC and were conducted in accordance with institutional guidelines and the NIH Guide for the Care and Use of Laboratory Animals.

Cell lines and cell culture

Human ESCC cell lines (KYSE30, KYSE70, TE10, and TE30) were obtained from the Cell Bank of the Chinese Academy of Sciences (Shanghai, China). The immortalized normal

esophageal epithelial cell line Het-1A was purchased from the American Type Culture Collection (ATCC, Manassas, VA, USA). All ESCC cell lines were cultured in RPMI-1640 medium (Gibco) supplemented with 10% fetal bovine serum (FBS) and 1% penicillin-streptomycin. In contrast, Het-1A cells were maintained in bronchial epithelial growth medium (BEGM; Lonza, Basel, Switzerland). Additionally, 293T cells, a human embryonic kidney cell line, were acquired from ATCC and cultured in DMEM medium (Gibco) containing 10% FBS. All cells were incubated at 37°C in a humidified atmosphere containing 5% CO_2. Cell line authentication was performed using short tandem repeat (STR) profiling, and all cell lines were confirmed to be free of Mycoplasma contamination.

Bioinformatic analysis

Transcriptomic profiles and corresponding clinical data of ESCC patients were obtained from the The Cancer Genome Atlas (TCGA) database. KDM4D mRNA levels were analyzed in 95 ESCC tissues and 11 normal esophageal tissues. Kaplan-Meier analysis was adopted to evaluate the prognostic value of KDM4D with respect to overall survival (OS). Based on the optimal cut-off, patients were stratified into high (0.28-4.04) and low (-1.10-0.27) KDM4D expression groups. The correlation between KDM4D with SRBD1 expression was examined using Spearman's correlation analysis. Chromosome segregation-related genes that correlated with KDM4D were identified and further categorized into functional groups, including kinetochore/centromere, decatenation, and spindle organization. H3K9me3 chromatin immunoprecipitation sequencing (ChIP-seq) data from HCT116 cells were analyzed to identify potential KDM4D binding sites within the SRBD1 intron 1 region (chr2: 45,610,800-45,611,200 bp).

Plasmid construction and cell transfection

The pLVX-Puro lentiviral vector encoding the full-length human KDM4D coding sequence (CCDS 8302.1) was synthesized by IBSBIO (Shanghai, China) for overexpression assays. The pLKO.1 vector was utilized to construct KDM4D-specific short hairpin RNAs (shRNAs) for gene silencing. The target sequence for sh-KDM4D was 5'-CCCTAAGTCCATTACCTCATA-3'. Control vectors included an empty pLVX-Puro vector and a scrambled shRNA (sh-Scr; target sequence: 5'-CCTAAGGTTAAGTCGCCCTCG-3'), which exhibited no significant homology to any known human gene, as confirmed by BLAST search. Similarly, overexpression and knockdown constructs targeting c-Myc (coding sequence: CCDS 6359.2; sh-c-Myc: 5'-CTGAGACAGATCAGCAACAA-3') and SRBD1 (coding sequence: CCDS 1823.1; sh-SRBD1: 5'-GCATCAATCTACAGTGTCA-3') were generated by IBSBIO.

For the luciferase reporter assay, the SRBD1 intron 1 fragment containing the wild-type H3K9me3 site (chr2: 45,610,700-45,611,150) or with deletion of the H3K9me3 site (chr2: 45,610,900-45,611,150) was synthesized and cloned into the pGL3-Basic vector (IBSBIO, Shanghai, China). Lentiviral particles were generated by co-transfecting 293T cells with transfer vectors and packaging plasmids (psPAX2 and pMD2.G) using Lipofectamine 3000 (Invitrogen) reagent. Viral supernatants were harvested at 48-72 hours post-transfection, filtered, and used to infect target cells in the presence of 8 μg/mL polybrene. Stable monoclonal cell lines were established through selection with 2 μg/mL puromycin for 7 to 10 consecutive days.

RNA extraction and quantitative real-time PCR (qRT-PCR)

Total RNA was extracted from cells using TRIzol reagent (Invitrogen) according to the manufacturer's instructions. RNA concentration and purity were determined using a NanoDrop spectrophotometer (Thermo Fisher Scientific, Waltham, MA, USA). Subsequently, 1 μg of total RNA was subjected to reverse transcription to generate complementary DNA (cDNA) using the PrimeScript RT Reagent Kit (Takara, Dalian, China). Quantitative real-time PCR (qRT-PCR) was conducted on an ABI 7500 Real-Time PCR System with SYBR Green Master Mix (Applied Biosystems). Relative mRNA expression was normalized to β-actin and calculated using the $2^{-\Delta\Delta Ct}$ approach. All experiments were performed in triplicate. Primer sequences are listed in Supplementary Table 1.

Western blot analysis

Cells and tissue samples were lysed in RIPA buffer (Beyotime, Shanghai, China) containing protease and phosphatase inhibitors (Roche, Basel, Switzerland). Protein concentrations

were determined using a BCA Protein Assay Kit. Equal amounts of protein (30-50 μg) were separated by SDS-PAGE and transferred onto PVDF membranes (Millipore, Billerica, MA, USA). Membranes were blocked with 5% non-fat milk diluted in TBST at room temperature for 1 h, followed by incubation with primary antibodies at 4°C overnight. The primary antibodies applied in this study were as follows: anti-KDM4D (Proteintech, 22591-1-AP, 1:500 for WB, 1:200 for IHC), anti-SRBD1 (Proteintech, 24931-1-AP, 1:1000), anti-RPL11 (Proteintech, 16277-1-AP, 1:500), anti-c-Myc (CST, #9402, 1:1000), anti-WIP1/PPM1D (Abcam, ab31270, 1:1000), anti-CHK1 (CST, #2360, 1:1000), anti-phospho-CHK1 (Ser345) (CST, #2348, 1:1000), anti-γH2AX (CST, #9718, 1:1000), anti-cleaved caspase-3 (CST, #9664, 1:1000), anti-cleaved PARP (CST, #5625, 1:1000), anti-BAX (CST, #2772, 1:1000), anti-H3K9me3 (Abcam, ab8898, 1:1000), and anti-β-actin (Proteintech, 66009-1-Ig, 1:5000). Following washing, the membranes were incubated with HRP-labeled secondary antibodies at room temperature for 1 hour. Protein bands were visualized using an ECL detection system (Millipore), with ImageJ being used for densitometric quantification.

Immunohistochemistry (IHC)

Formalin-fixed, paraffin-embedded (FFPE) tissue sections (4 μm) were deparaffinized in xylene, followed by rehydration with graded ethanol. Antigen retrieval was performed by microwave heating in citrate buffer (pH 6.0) for 20 min, and 3% hydrogen peroxide was used to quench endogenous peroxidase activity for 15 min. Sections were then blocked with 5% normal goat serum for 30 min and then incubated with anti-KDM4D antibody (Proteintech, 22591-1-AP, 1:200) or anti-Ki67 antibody (Abcam, ab16667, 1:200) overnight at 4°C. After washing, sections were incubated with HRP-conjugated secondary antibody and developed using DAB substrate. Sections were counterstained with hematoxylin, dehydrated, and mounted. Immunoreactivity was quantified using the H-score method: H-score = Σ (intensity × percentage), where staining intensity ranges from 0 (negative) to 3 (strong positive), and percentage represents the proportion of positive cells at each intensity level. Images were captured at 10× and 40× magnification.

TUNEL assay

Apoptotic cells were detected using a TUNEL assay kit (In Situ Cell Death Detection Kit, Roche), following the manufacturer's instructions. After fixation in 4% paraformaldehyde and permeabilization in 0.1% Triton X-100, specimens were incubated with TUNEL reagent at 37°C for 1 hour in the dark, and DAPI was used for nuclear counterstaining. Fluorescence images were acquired using a Nikon fluorescence microscope (Nikon, Tokyo, Japan), and the percentage of TUNEL-positive cells was quantified in at least five randomly selected fields for each sample.

Cell viability and LDH release assays

Cell viability was evaluated using a CCK-8 assay kit (Dojindo, Kumamoto, Japan). Cells were seeded into 96-well plates and subjected to the indicated treatments. 10 μL CCK-8 solution was added to each well, followed by incubation at 37°C for 2 hours at corresponding time points. Absorbance at 450 nm was measured using a microplate reader (Bio-Rad). Lactate dehydrogenase (LDH) release was assessed using a detection kit (Beyotime, Shanghai, China) according to the manufacturer's protocol, and the activity was expressed as fold change relative to the control group.

Irradiation treatment

Cells were irradiated using a linear accelerator (Varian, Palo Alto, CA, USA) at a dose rate of 2 Gy per minute. For *in vitro* experiments, cells were exposed to a single dose of 4 Gy and harvested at 0, 1, 6, and 12 h post-irradiation for subsequent analyses. For xenograft experiments, tumor-bearing mice received a single dose of 10 Gy localized irradiation to the tumor region.

Chromatin immunoprecipitation (ChIP) and RNA immunoprecipitation (RIP)

ChIP assays were performed using the SimpleChIP Enzymatic Chromatin IP Kit (CST) in strict accordance with the manufacturer's protocols. Briefly, cells were cross-linked with 1% formaldehyde, lysed, and chromatin was fragmented by enzymatic digestion. The chromatin was immunoprecipitated using antibodies against KDM4D (Proteintech, 22591-1-AP),

H3K9me3 (Abcam, ab8898), or normal IgG as a negative control. The extracted DNA was purified and subjected to PCR amplification using primers targeting the SRBD1 intron 1 region, generating a 137 bp amplicon. The β-actin promoter served as a negative control (250 bp amplicon). RIP assays were implemented using the Magna RIP Kit (Millipore). Briefly, cells were lysed in RIP lysis buffer, and RNA-protein complexes were immunoprecipitated with KDM4D-specific antibody or IgG. Co-precipitated RNA was extracted and analyzed by RT-PCR to detect RPL11 mRNA (126 bp amplicon), with β-actin mRNA (250 bp amplicon) serving as a control.

Dual-luciferase reporter assay

293T cells were seeded into 24-well plates and co-transfected with pGL3-SRBD1 intron 1 reporter plasmids (either wild-type or H3K9me3 site-deleted mutants), along with the pRL-TK Renilla luciferase plasmid as internal control, and either a KDM4D overexpression plasmid or the corresponding empty control vector. Transfections were performed using Lipofectamine 3000 (Invitrogen) according to the manufacturer's instructions. At 48 h post-treatment, cells were lysed and luciferase activity were measured using the Dual-Luciferase Reporter Assay System (Promega). Renilla luciferase activity served as the internal reference to normalize firefly luciferase activity, and the relative values were calculated as fold change over the control.

Xenograft tumor model

All animal procedures were approved by the Institutional Animal Care and Use Committee (IACUC) of The First Affiliated Hospital of USTC and were conducted in compliance with the relevant institutional animal care regulations. Female BALB/c nude mice (4-6 weeks, 18-20 g) were obtained from Beijing Vital River Laboratory Animal Technology Co., Ltd. and maintained in SPF conditions with *ad libitum* access to food and water. For xenograft tumor formation assays, 5×10^6 genetically modified KYSE70 or TE10 cells were resuspended in 100 μL PBS and subcutaneously inoculated into the right flank of nude mice. Once tumor volumes reached approximately 100 mm^3, the animals were randomly allocated to the indicated treatment groups (n = 6 per group) and received either local irradiation (10 Gy) or no treatment. Tumor volume was measured every 3 days using a digital caliper and calculated according to the formula: volume = (length × $width^2$)/2. Mouse body weight was monitored every 3 days throughout the experiment. On day 21 following irradiation, mice were euthanized by carbon dioxide (CO_2) inhalation at a flow rate of 30% of the cage volume per minute, in accordance with the 2020 AVMA Guidelines for the Euthanasia of Animals. Animal death was verified by cessation of respiration, absence of heartbeat, and loss of pedal withdrawal reflex. Tumors were then excised, weighed, photographed, and processed for histological and molecular analyses. All tumor measurements and data analysis were conducted in a blinded fashion to minimize observer bias.

Statistical analysis

Statistical analyses were performed using GraphPad Prism 9.0 and SPSS 25.0 software. Data were presented as mean ± standard deviation (SD) from three independent experiments. Comparisons between two groups were performed using an unpaired two-tailed Student's t-test, while one-way analysis of variance (ANOVA) followed by Tukey's post hoc test was applied for multiple-group comparisons. Survival curves were generated using the Kaplan-Meier method, and differences were evaluated by the log-rank test. Receiver operating characteristic (ROC) curve analysis was performed to evaluate the predictive performance of KDM4D expression (H-score) for radiotherapy response (TRG 0-1 vs. TRG 2-3). The area under the ROC curve (AUC) and corresponding 95% confidence intervals (CIs) were calculated, and the optimal cutoff value was determined using the Youden index. The correlation between KDM4D expression and clinicopathologic features was analyzed using the chi-square test. A P-value < 0.05 was considered significant, with significance levels denoted as $*P < 0.05$, $**P < 0.01$, and $***P < 0.001$.

Results

KDM4D was overexpressed in ESCC and its high expression correlated with improved overall survival

To evaluate KDM4D expression in ESCC, we first assessed its mRNA levels using transcriptomic data from TCGA database. KDM4D

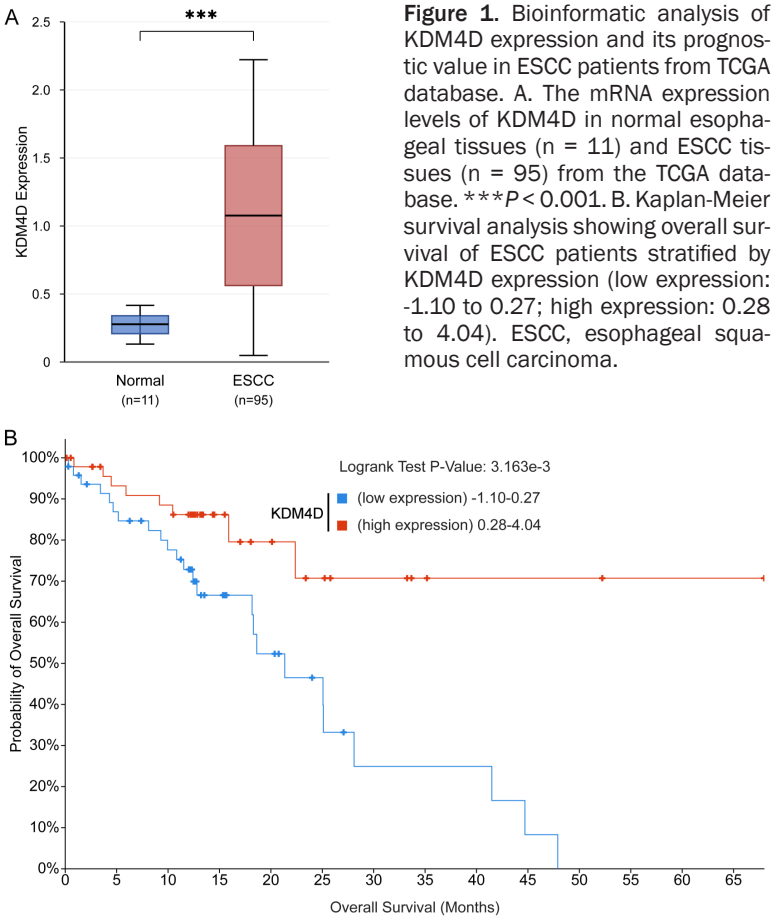

Figure 1. Bioinformatic analysis of KDM4D expression and its prognostic value in ESCC patients from TCGA database. A. The mRNA expression levels of KDM4D in normal esophageal tissues (n = 11) and ESCC tissues (n = 95) from the TCGA database. ***$P < 0.001$. B. Kaplan-Meier survival analysis showing overall survival of ESCC patients stratified by KDM4D expression (low expression: -1.10 to 0.27; high expression: 0.28 to 4.04). ESCC, esophageal squamous cell carcinoma.

expression was significantly elevated in 95 ESCC tissues compared with 11 normal esophageal tissues (**Figure 1A**). Kaplan-Meier analysis demonstrated that ESCC patients with low KDM4D expression had significantly poorer overall survival than those with high expression (Log-rank test, $P = 3.163 \times 10^{-3}$; **Figure 1B**). Collectively, these findings indicate that KDM4D is overexpressed in ESCC and may serve as a prognostic biomarker.

High KDM4D expression predicted favorable response to neoadjuvant radiotherapy

To explore the correlation between KDM4D expression and radiotherapy response, we analyzed tissue specimens from 32 ESCC patients receiving neoadjuvant chemoradiotherapy. Patients were stratified into a favorable response group (TRG 0-1, n = 11) and a non-response group (TRG 2-3, n = 21) according to pathologic tumor regression grading.

The clinicopathologic features of the enrolled patients are summarized in **Table 1**. No significant intergroup differences were detected with regard to age, sex, tumor location, tumor length, differentiation grade, Union for International Cancer Control (UICC) stage, or lymph node metastasis. Notably, KDM4D expression was significantly correlated with radiotherapy response ($P = 0.035$). IHC analysis revealed that patients with a favorable response exhibited markedly higher KDM4D H-scores than non-responders ($P = 0.035$; **Figure 2A**). Representative IHC images displayed robust nuclear KDM4D staining in responsive tumors (TRG 0-1) and faint staining in non-responsive tumors (TRG 2-3) (**Figure 2A**). Consistently, the majority of patients with high KDM4D expression (n = 9) achieved a favorable response, whereas most cases with low KDM4D expression (n = 23) exhibited treatment resistance ($P = 0.035$; **Figure 2B**). Moreover, Kaplan-Meier analysis demonstrated that high KDM4D expression was associated with prolonged PFS ($P = 0.045$; **Figure 2C**). ROC curve analysis was performed to evaluate the predictive value of KDM4D expression (H-score) for distinguishing responders from non-responders. The AUC was 0.73 (95% CI: 0.54-0.92; $P = 0.035$), and the optimal cutoff value determined by the Youden index was 115, yielding a sensitivity of 72.7% and a specificity of 71.4% (**Table 1**). These results indicate that KDM4D expression may serve as a predictive biomarker for radiotherapy response in ESCC.

KDM4D knockdown enhanced radioresistance in ESCC cells both in vitro and in vivo

We first examined KDM4D expression in a panel of ESCC cell lines. Western blot and qRT-PCR analyses demonstrated that KYSE70 cells exhibited the highest KDM4D expression, whereas TE10 cells showed relatively lower expression compared to the normal esophageal epithelial cell line Het-1A (**Figure 3A**, **3B**). Therefore, KYSE70 cells were selected for

Table 1. Clinicopathologic characteristics of ESCC patients according to response to neoadjuvant radiotherapy

Characteristic	Response (n = 11)	Non-response (n = 21)	*P* value
Age (years), mean ± SD	57.8 ± 7.2	58.0 ± 5.9	0.955
Gender			0.053
Male	4 (36.4%)	16 (76.2%)	
Female	7 (63.6%)	5 (23.8%)	
Tumor location			0.206
Upper	0 (0.0%)	5 (23.8%)	
Middle	5 (45.5%)	8 (38.1%)	
Lower	6 (54.5%)	8 (38.1%)	
Tumor length (cm), mean ± SD	4.7 ± 1.5	4.6 ± 1.2	0.850
Differentiation			0.497
Well	2 (18.2%)	8 (38.1%)	
Moderate	6 (54.5%)	8 (38.1%)	
Poor	3 (27.3%)	5 (23.8%)	
UICC Stage			0.712
Stage II	5 (45.5%)	12 (57.1%)	
Stage III	6 (54.5%)	9 (42.9%)	
Lymph node metastasis			0.266
Positive	7 (63.6%)	8 (38.1%)	
Negative	4 (36.4%)	13 (61.9%)	
KDM4D expression			0.035*
High	6 (54.5%)	3 (14.3%)	
Low	5 (45.5%)	18 (85.7%)	

Abbreviations: ESCC, esophageal squamous cell carcinoma; TRG, tumor regression grade; UICC, Union for International Cancer Control; KDM4D, lysine-specific demethylase 4D; SD, standard deviation. TRG 0-1; Non-response: TRG 2-3. ROC curve analysis for KDM4D H-score predicting radiotherapy response: AUC = 0.73 (95% CI: 0.54-0.92; *P* = 0.035); optimal cutoff (Youden index): H-score = 115, sensitivity = 72.7%, specificity = 71.4%. **P* < 0.05 was considered statistically significant.

KDM4D knockdown experiments and TE10 cells for overexpression studies.

To investigate the role of KDM4D in radiosensitivity, KYSE70 cells with stable KDM4D knockdown (sh-KDM4D) or control shRNA (sh-Scr) were exposed to 4 Gy irradiation and analyzed at the indicated time points. TUNEL staining revealed that KDM4D knockdown significantly reduced radiation-induced apoptosis compared to control cells, with the difference becoming more pronounced at 6 and 12 h post-irradiation (**Figure 3C**, **3D**). Consistently, KDM4D knockdown increased cell viability and decreased LDH release following irradiation (**Figure 3D**). Western blot analysis further showed that, upon irradiation, sh-KDM4D cells exhibited increased protein levels of c-Myc, WIP1, and CHK1, accompanied by decreased levels phosphorylated CHK1 (Ser345), γH2AX, cleaved caspase-3, and cleaved PARP compared to control cells (**Figure 3E**; Supplementary Figure 1A). Notably, BAX expression remained unchanged (**Figure 3E**), consistent with the TP53-mutant status of KYSE70 cells [17], as BAX is a direct transcriptional target of p53 and its expression is dependent on functional p53 [18, 19].

To validate these findings *in vivo*, xenograft tumors were established using KYSE70 cells transduced with sh-Scr or sh-KDM4D. When tumors reached approximately 100 mm^3, mice were randomly assigned to receive local irradiation (10 Gy) or no treatment. On day 21 post-irradiation, tumors in the sh-KDM4D group exhibited significantly increased tumor weight compared with the sh-Scr group following radiation treatment, whereas the untreated group displayed larger tumor sizes (**Figure 3F**). Western blot analysis of tumor tissues confirmed the molecular changes observed *in vitro*, with sh-KDM4D tumors showing reduced levels of p-CHK1, γH2AX, cleaved caspase-3, and

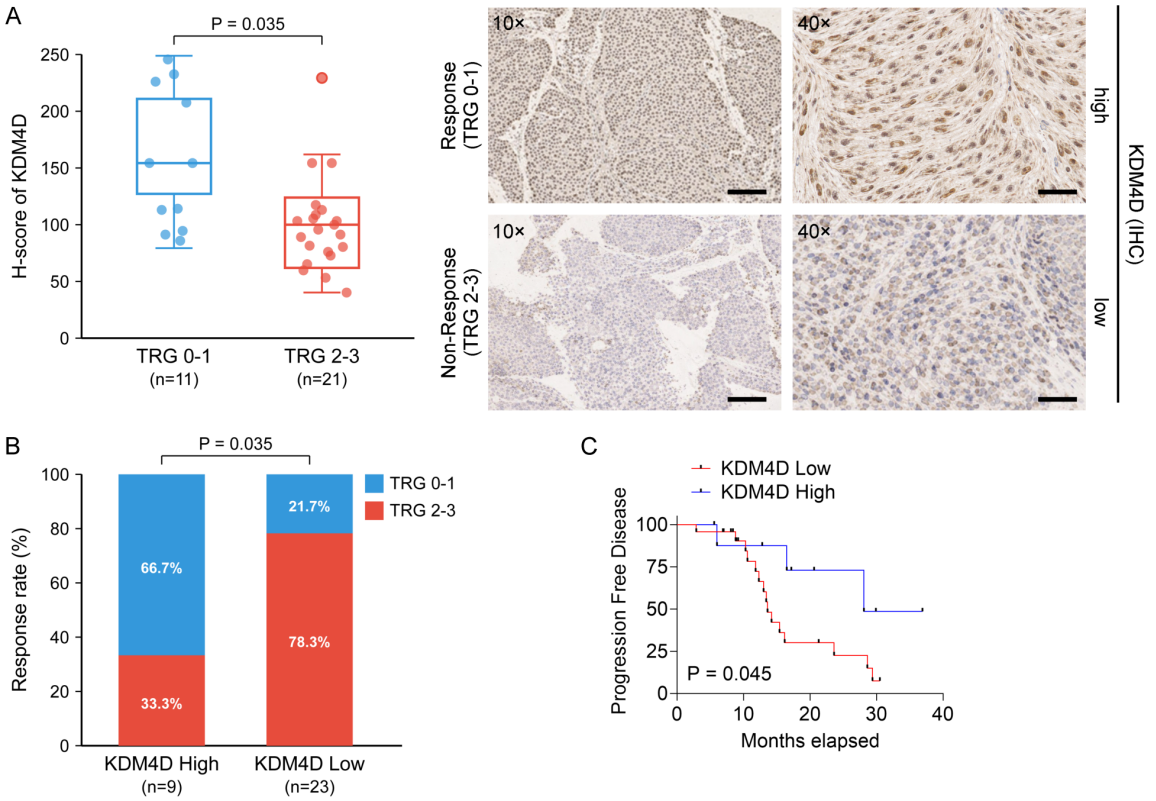

Figure 2. Clinical correlation between KDM4D expression and neoadjuvant chemoradiotherapy response in ESCC patients. A. Left panel: Quantification of KDM4D H-score in ESCC patients with favorable response (TRG 0-1, n = 11) and non-response (TRG 2-3, n = 21) to neoadjuvant radiotherapy; Right panel: Representative immunohistochemical staining of KDM4D in responders and non-responders at 10× (Scale bar = 50 μm) and 40× (Scale bar = 200 μm) magnification. B. Distribution of tumor regression grades in patients with high (n = 9) versus low (n = 23) KDM4D expression. C. Kaplan-Meier curves showing progression-free survival of ESCC patients stratified by KDM4D expression.

cleaved PARP after irradiation (**Figure 3G**; Supplementary Figure 1B). Furthermore, IHC and TUNEL staining demonstrated an increase in Ki67-positive proliferating cells and a decrease in apoptotic cells in irradiated sh-KDM4D tumors compared to irradiated sh-Scr tumors (**Figure 3H**). These results demonstrate that KDM4D knockdown promotes radioresistance in ESCC cells both *in vitro* and *in vivo*.

KDM4D activated SRBD1 transcription through H3K9me3 demethylation at its intron 1

To identify downstream targets of KDM4D, we analyzed genes correlated with KDM4D expression in the TCGA ESCC dataset. Among chromosome segregation-related genes, SRBD1 exhibited a significant positive correlation with KDM4D (**Figure 4A**). Importantly, Kaplan-Meier analysis indicated that elevated SRBD1 expression was associated with improved overall survival in ESCC patients (Log-rank test, $P = 0.024$; **Figure 4B**), consistent with the prognostic pattern observed for KDM4D. Additionally, correlation analysis validated a significant positive association between KDM4D and SRBD1 expression ($r = 0.368$, $P = 0.00024$; **Figure 4C**).

Analysis of ChIP-seq data from HCT116 cells [20] revealed an H3K9me3-enriched region within intron 1 of the SRBD1 gene (chr2: 45,610,800-45,611,200 bp) (**Figure 4D**). To determine whether KDM4D regulates SRBD1 transcription through H3K9me3 demethylation, dual-luciferase reporter assays were performed in 293T cells. Constructs containing either the wild-type SRBD1 intron 1 harboring the H3K9me3 site (chr2: 45,610,700-45,611,150) or a deletion of this site (chr2: 45,610,900-45,611,150) were generated. KDM4D overexpression significantly increased

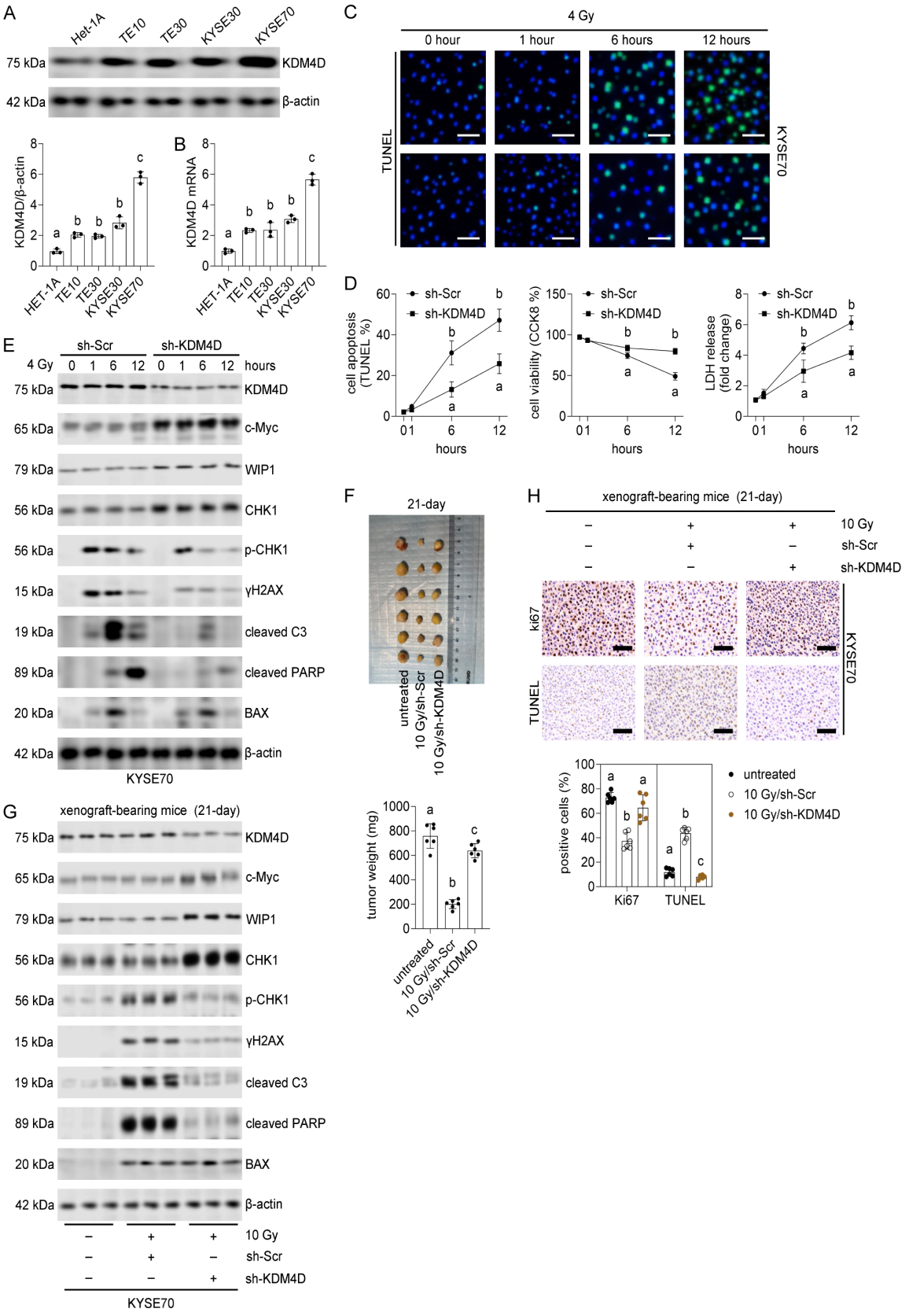
A
Het-1A
TE10
TE30
KYSE30
KYSE70
75 kDa
KDM4D
42 kDa
β-actin
KDM4D/β-actin
B
KDM4D mRNA
C
4 Gy
0 hour
1 hour
6 hours
12 hours
TUNEL
KYSE70
D
sh-Scr
sh-KDM4D
cell apoptosis (TUNEL %)
cell viability (CCK8 %)
LDH release (fold change)
hours
E
sh-Scr
sh-KDM4D
4 Gy
0 1 6 12 0 1 6 12 hours
75 kDa KDM4D
65 kDa c-Myc
79 kDa WIP1
56 kDa CHK1
56 kDa p-CHK1
15 kDa γH2AX
19 kDa cleaved C3
89 kDa cleaved PARP
20 kDa BAX
42 kDa β-actin
KYSE70
F
21-day
untreated
10 Gy/sh-Scr
10 Gy/sh-KDM4D
tumor weight (mg)
G
xenograft-bearing mice (21-day)
75 kDa KDM4D
65 kDa c-Myc
79 kDa WIP1
56 kDa CHK1
56 kDa p-CHK1
15 kDa γH2AX
19 kDa cleaved C3
89 kDa cleaved PARP
20 kDa BAX
42 kDa β-actin
10 Gy
sh-Scr
sh-KDM4D
KYSE70
H
xenograft-bearing mice (21-day)
10 Gy
sh-Scr
sh-KDM4D
ki67
TUNEL
KYSE70
positive cells (%)
Ki67
TUNEL
untreated
10 Gy/sh-Scr
10 Gy/sh-KDM4D

Figure 3. Effects of KDM4D knockdown on radiation-induced apoptosis and DNA damage response in ESCC cells and xenograft tumors. A. Western blot analysis (upper) and quantification (lower) of KDM4D protein expression in normal esophageal epithelial cell line Het-1A and ESCC cell lines (TE10, TE30, KYSE30 and KYSE70). β-actin served as loading control. The same letter indicates no significant difference between groups, while different letters indicate significant differences between groups. B. qRT-PCR analysis of KDM4D mRNA expression in the indicated cell lines. C. Representative TUNEL staining images showing apoptosis in KYSE70 cells with sh-Scr (upper) or sh-KDM4D (lower) at 0, 1, 6 and 12 hours after 4 Gy irradiation. Scale bar = 50 μm. D. Quantification of TUNEL-positive cells (left), cell viability assessed by CCK-8 assay (middle), and LDH release (right) in sh-Scr and sh-KDM4D KYSE70 cells at indicated time points after 4 Gy irradiation (n = 3). The same letter indicates no significant difference between groups, while different letters indicate significant differences between groups. E. Western blot analysis of KDM4D, c-Myc, WIP1, CHK1, p-CHK1, γH2AX, cleaved caspase-3, cleaved PARP and BAX in KYSE70 cells with sh-Scr or sh-KDM4D at indicated time points after 4 Gy irradiation. β-actin served as loading control. F. Upper: Representative images of xenograft tumors at day 21. Lower: Quantification of tumor weights (n = 6 per group). The same letter indicates no significant difference between groups, while different letters indicate significant differences between groups. G. Western blot analysis of the indicated proteins in xenograft tumor tissues from untreated, 10 Gy/sh-Scr and 10 Gy/sh-KDM4D groups (n = 3 per group). H. Representative immunohistochemical staining of Ki67 (upper) and TUNEL staining (lower) in xenograft tumor sections at day 21 post-irradiation from the indicated treatment groups. Scale bar = 200 μm. Lower panel, Quantification of Ki67-positive cells (left) and TUNEL-positive cells (right) from at least five random high-power fields per section in untreated, 10 Gy/sh-Scr and 10 Gy/sh-KDM4D groups (n = 6 per group). The same letter indicates no significant difference between groups, while different letters indicate significant differences between groups. ESCC, esophageal squamous cell carcinoma.

luciferase activity of the wild-type construct, whereas this effect was abolished upon deletion of the H3K9me3 site (**Figure 4E**).

ChIP-PCR experiments in KYSE70 and TE10 cells further validated these findings. KDM4D knockdown in KYSE70 cells resulted in increased H3K9me3 enrichment at SRBD1 intron 1, whereas KDM4D overexpression in TE10 cells decreased H3K9me3 levels (**Figure 4F**). These data indicate that KDM4D promotes SRBD1 transcription by mediating H3K9me3 demethylation at its intron 1 region.

KDM4D regulated the SRBD1/RPL11/c-Myc/WIP1/CHK1 signaling axis

Given that KDM4D positively regulates SRBD1 expression, and considering previous reports that SRBD1 regulates RPL11 expression and exerts suppressive effects through the RPL11-MDM2-p53 pathway [16], as well as evidence that RPL11 negatively regulates c-Myc and influences chemotherapy sensitivity in breast cancer [21], we hypothesized that KDM4D may regulate radiosensitivity through the SRBD1/RPL11/c-Myc pathway.

RIP-PCR analysis demonstrated KDM4D manipulation affected RPL11 mRNA expression, consistent with the role of SRBD1 in regulating RPL11 expression (**Figure 4G**). Comparison between TE10 (low KDM4D expression) and KYSE70 (high KDM4D expression) cells revealed that KYSE70 cells exhibited higher levels of SRBD1 and RPL11, accompanied by lower levels of c-Myc, WIP1, and CHK1 at both the protein and mRNA levels (**Figure 5A**, **5B**). These findings support a regulatory cascade in which KDM4D positively regulates SRBD1 and RPL11, which in turn suppress c-Myc and its downstream targets WIP1 and CHK1.

To confirm this regulatory axis, gain- and loss-of-function experiments were performed. KDM4D overexpression in TE10 cells increased SRBD1 and RPL11 expression while decreasing c-Myc, WIP1, and CHK1 levels. Conversely, KDM4D knockdown in KYSE70 cells exerted the opposite effects (**Figure 5C**, **5D**). These changes were observed at both the protein and mRNA levels, suggesting transcriptional regulation. Collectively, these results establish that KDM4D regulates the SRBD1/RPL11/c-Myc/WIP1/CHK1 signaling axis, providing a mechanistic basis for its role in modulating radiosensitivity.

c-Myc mediated KDM4D-regulated radiosensitivity in ESCC cells

To determine whether c-Myc functions as a critical mediator of KDM4D-regulated radiosensitivity, rescue experiments were performed. In TE10 cells, KDM4D overexpression alone enhanced radiation-induced apoptosis, as reflected by an increase in the proportion of TUNEL-positive cells, reduced cell viability, and elevated LDH release (**Figure 6A**, **6B**). These effects were markedly attenuated upon co-overexpression of c-Myc. Conversely, in KYSE70 cells, KDM4D knockdown reduced radiation-

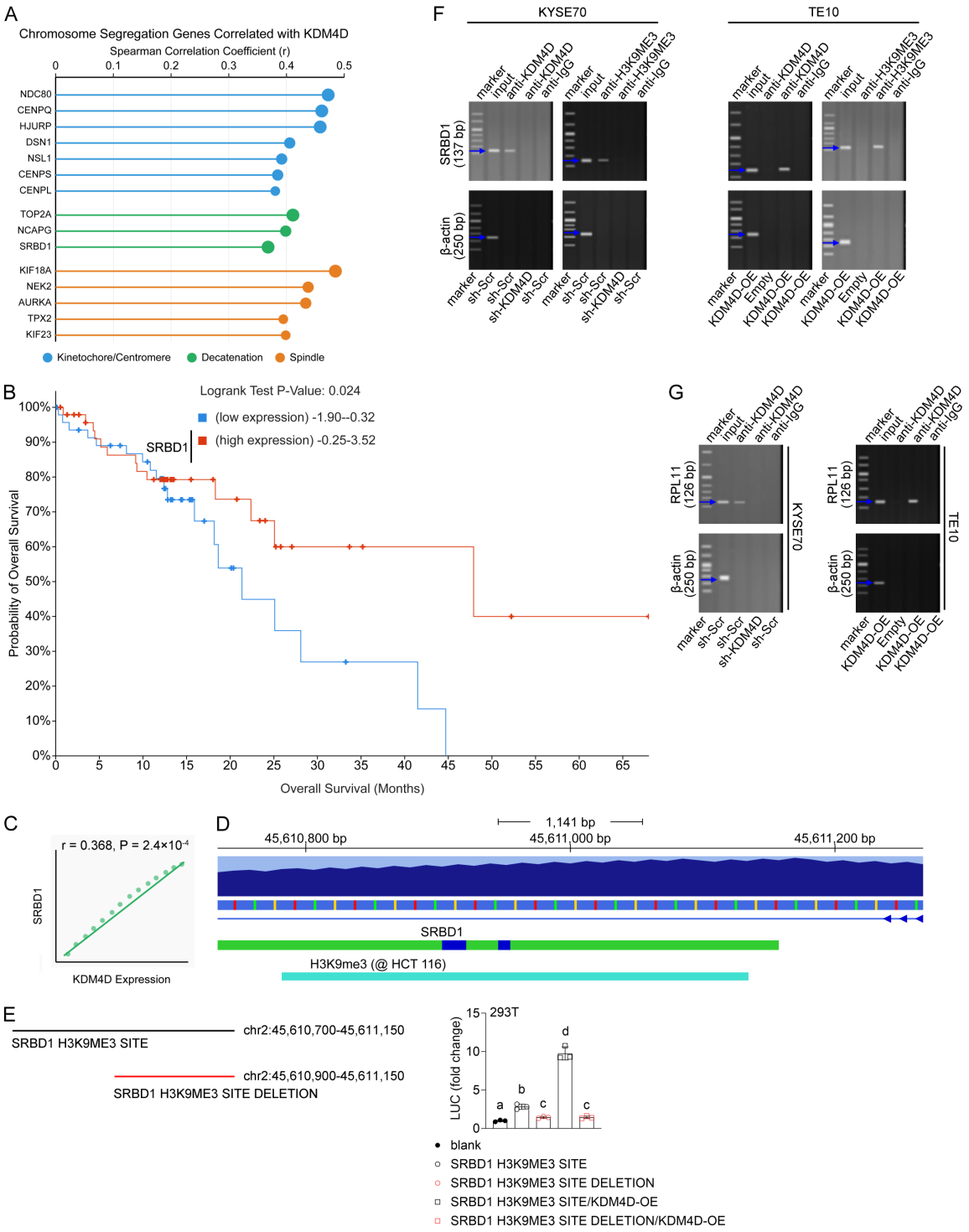

Figure 4. Identification of SRBD1 as a direct transcriptional target of KDM4D through H3K9me3 demethylation. A. Chromosome segregation genes correlated with KDM4D expression, including kinetochore/centromere components (blue), decatenation factors (green), and spindle regulators (orange). SRBD1 is among the top correlated genes. B. Kaplan-Meier survival analysis of ESCC patients stratified by SRBD1 expression (low expression: -1.90 to 0.32; high expression: -0.25 to 3.52). Log-rank test $P = 0.024$. C. Correlation analysis between KDM4D and SRBD1 mRNA expression in TCGA ESCC dataset ($r = 0.368$, $P = 2.4 \times 10^{-4}$). D. Schematic representation of the SRBD1 gene locus (chr2: 45,610,800-45,611,200 bp) showing the H3K9me3 modification site based on ChIP-seq data from HCT116 cells. E. Left: Schematic of SRBD1 intron 1 luciferase constructs containing the wild-type H3K9me3 site (chr2: 45,610,700-45,611,150) or deletion of the H3K9me3 site (chr2: 45,610,900-45,611,150). Right: Dual-

luciferase reporter assay in 293T cells showing SRBD1 intron 1 activity under different conditions. The same letter indicates no significant difference between groups, while different letters indicate significant differences between groups (n = 3). F. ChIP-PCR analysis of SRBD1 intron 1 (137 bp) and β-actin control (250 bp) in KYSE70 cells with sh-Scr or sh-KDM4D (left panels) and TE10 cells with empty vector or KDM4D-OE (right panels), immunoprecipitated with anti-KDM4D, anti-H3K9me3 or IgG antibodies. G. RIP-PCR analysis of RPL11 mRNA (126 bp) and β-actin control (250 bp) in KYSE70 cells with sh-Scr or sh-KDM4D (left panels) and TE10 cells with empty vector or KDM4D-OE (right panels).

induced apoptosis, enhanced cellular viability, and suppressed LDH release, and these effects were reversed by concurrent c-Myc knockdown (**Figure 6A**, **6B**). Western blot analysis further revealed the molecular mechanisms underlying these phenotypic changes. In TE10 cells, KDM4D overexpression downregulated c-Myc, WIP1, and CHK1 expression, accompanied by increased levels of p-CHK1 (Ser345), γH2AX, and cleaved caspase-3 (**Figure 6C**; Supplementary Figure 2A). In contrast, KDM4D knockdown in KYSE70 cells increased c-Myc, WIP1, and CHK1 expression, along with reduced levels of p-CHK1 (Ser345), γH2AX, and cleaved caspase-3 (**Figure 6C**; Supplementary Figure 2B). Collectively, these results confirm that c-Myc is an essential downstream effector of KDM4D in regulating radiosensitivity, likely through modulation of its downstream target genes.

SRBD1 mediated KDM4D-regulated radiosensitivity in ESCC cells

To further determine whether SRBD1 acts as the key downstream mediator connecting KDM4D to the c-Myc pathway, analogous rescue experiments were conducted. In TE10 cells, the radiosensitizing effect induced by KDM4D overexpression was attenuated by concurrent SRBD1 knockdown, as reflected by decreased TUNEL-positive cells, increased cell viability, and reduced LDH release (**Figure 6D**, **6E**). In KYSE70 cells, the radioresistance conferred by KDM4D knockdown was reversed by SRBD1 overexpression (**Figure 6D**, **6E**).

Western blot analysis demonstrated that SRBD1 knockdown in KDM4D-overexpressing TE10 cells restored the expression of c-Myc, WIP1, and CHK1, and attenuated the radiation-induced upregulation of p-CHK1, γH2AX, cleaved caspase-3, and cleaved PARP (**Figure 6F**; Supplementary Figure 3A). Conversely, SRBD1 overexpression in KDM4D-knockdown KYSE70 cells suppressed c-Myc, WIP1, and CHK1 levels, resulting in augmented radiation-triggered DNA damage and apoptosis (**Figure 6F**; Supplementary Figure 3B). These findings verify that SRBD1 serves as the critical mediator linking KDM4D to the c-Myc/WIP1/CHK1 axis in the regulation of ESCC radiosensitivity.

SRBD1 is required for KDM4D-mediated regulation of radiosensitivity in vivo

Finally, the role of KDM4D-SRBD1 axis was validated in xenograft models. In TE10 cell-derived xenografts, KDM4D overexpression significantly enhanced tumor radiosensitivity, as evidenced by reduced tumor weight following 10 Gy irradiation compared to the empty vector control group. However, this radiosensitizing effect was markedly attenuated when SRBD1 was simultaneously knocked down (**Figure 7A**, **7B**). Western blot analysis of tumor tissues further confirmed that KDM4D overexpression activated the SRBD1/RPL11 pathway while suppressing the c-Myc/WIP1/CHK1 axis, which in turn led to sustained activation of p-CHK1 and increased expression of apoptosis-related markers after irradiation. SRBD1 knockdown reversed these molecular changes (**Figure 7A**; Supplementary Figure 4A). Consistently, IHC and TUNEL staining showed that KDM4D-overexpressing tumors exhibited reduced Ki-67-positive proliferating cells and increased TUNEL-positive apoptotic cells after irradiation, and these effects were reversed by SRBD1 knockdown (**Figure 7C**). Quantitative analysis further confirmed statistically significant differences among the treatment groups (**Figure 7C**).

Complementary experiments using KYSE70 cell-derived xenografts yielded consistent results. KDM4D knockdown promoted radioresistance, as evidenced by increased tumor volumes following irradiation, whereas concurrent SRBD1 overexpression restored radiosensitivity (**Figure 7D**, **7E**). Molecular analysis confirmed the expected alterations in the SRBD1/RPL11/c-Myc/WIP1/CHK1/p-CHK1 signaling axis (**Figure 7D**; Supplementary Figure 4B). Moreover, Ki67 and TUNEL staining corrobo-

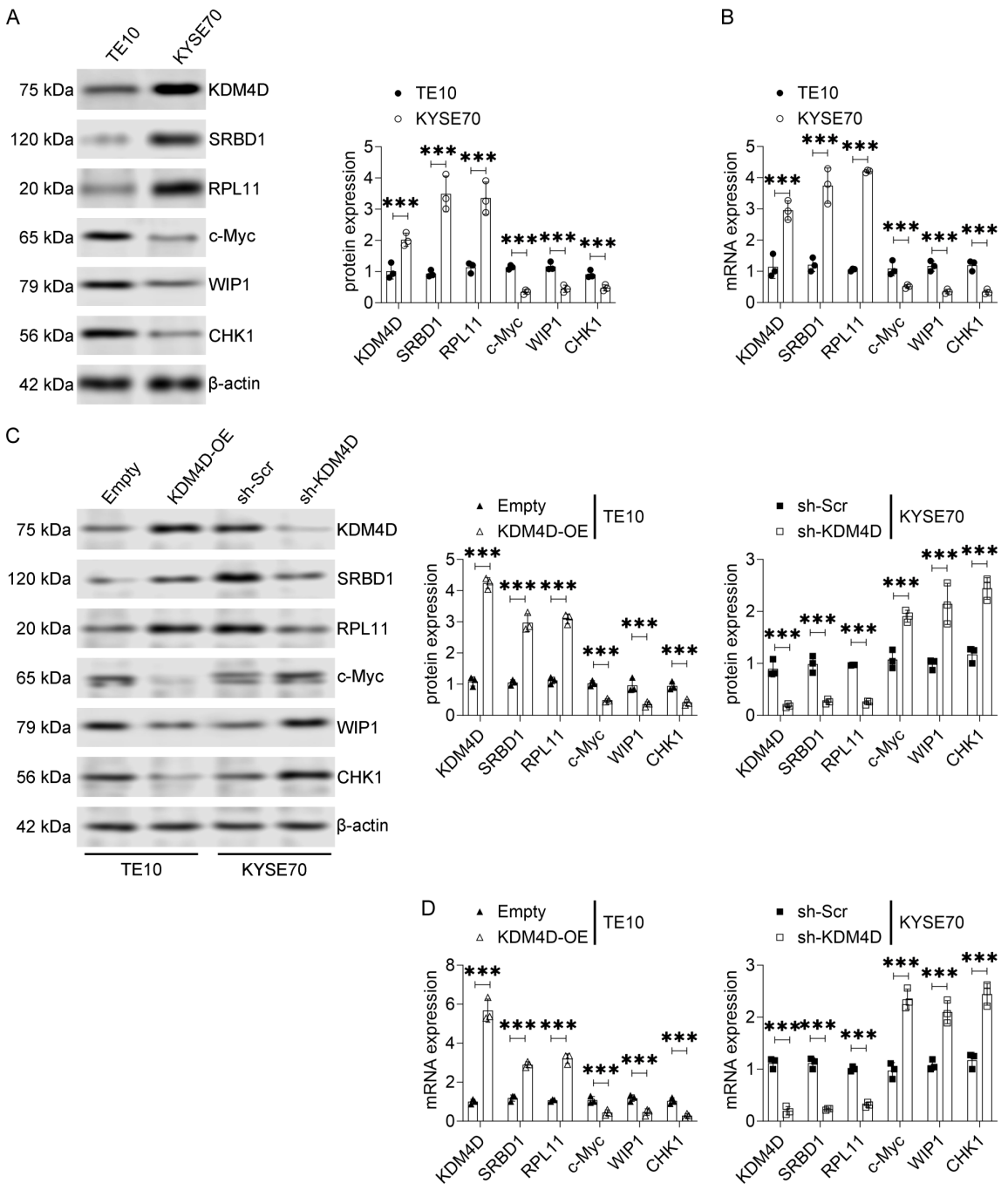

Figure 5. Expression analysis of the SRBD1/RPL11/c-Myc/WIP1/CHK1 pathway components upon KDM4D manipulation. A. Western blot analysis (left) and quantification (right) of KDM4D, SRBD1, RPL11, c-Myc, WIP1 and CHK1 protein expression in TE10 (low KDM4D) and KYSE70 (high KDM4D) cells (n = 3). ***$P < 0.001$. B. qRT-PCR analysis of the indicated genes in TE10 and KYSE70 cells (n = 3). ***$P < 0.001$. C. Western blot analysis (left) and quantification (right) of the indicated proteins in TE10 cells with empty vector or KDM4D-OE and KYSE70 cells with sh-Scr or sh-KDM4D (n = 3). ***$P < 0.001$. D. qRT-PCR analysis of the indicated genes in TE10 cells with empty vector or KDM4D-OE and KYSE70 cells with sh-Scr or sh-KDM4D (n = 3). ***$P < 0.001$.

rated the changes in cell proliferation and apoptosis, and quantitative analysis of these staining results revealed statistically significant differences that were consistent with the molecular findings (**Figure 7F**). Collectively, these *in vivo* data demonstrated that SRBD1 is essential for KDM4D-mediated regulation of radiosensitivity in ESCC.

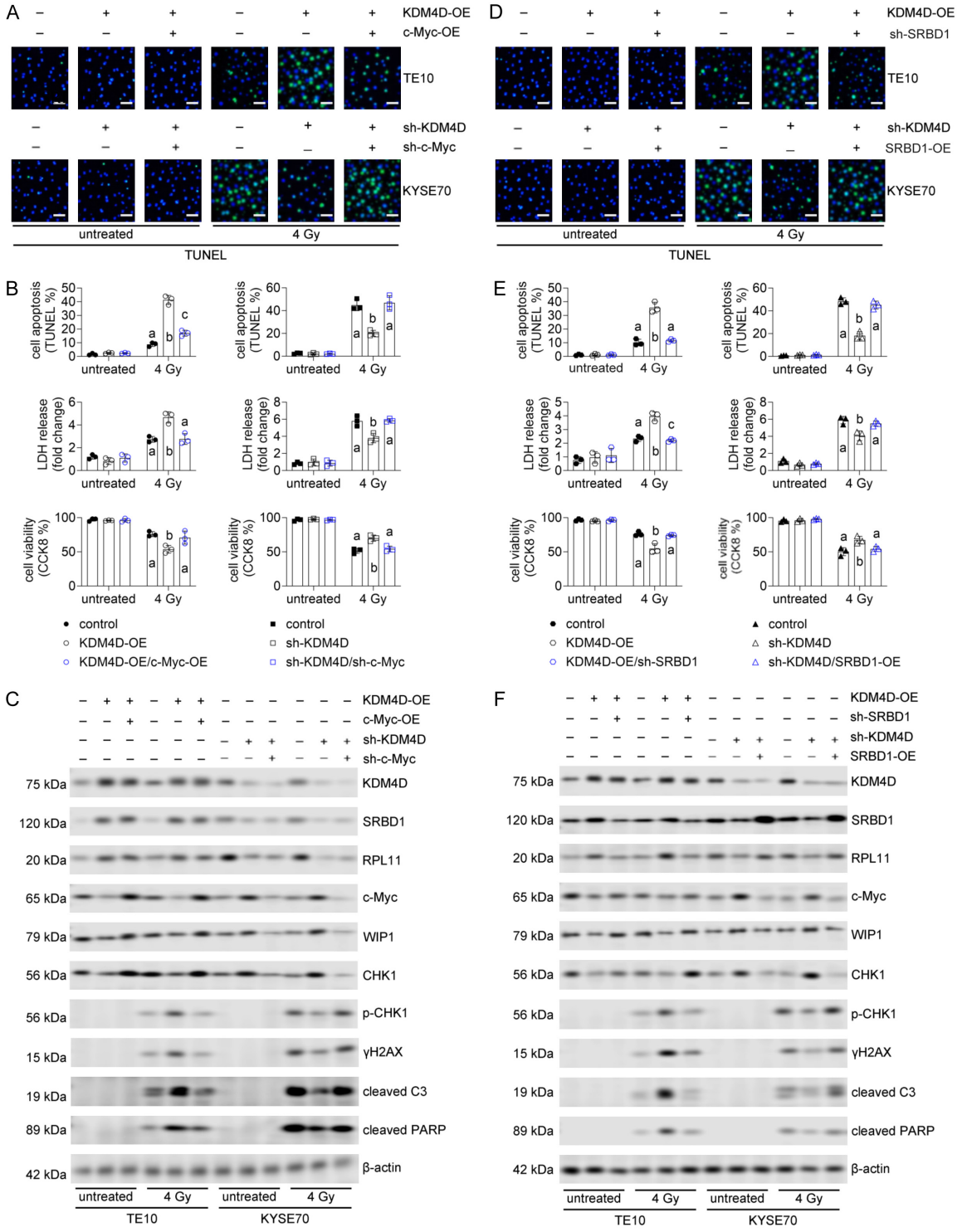

Figure 6. Rescue experiments validating c-Myc and SRBD1 as functional mediators of KDM4D-regulated radiosensitivity. A. Representative TUNEL staining images in TE10 cells (upper panels: control, KDM4D-OE, KDM4D-OE/c-Myc-OE) and KYSE70 cells (lower panels: control, sh-KDM4D, sh-KDM4D/sh-c-Myc) with or without 4 Gy irradiation. Scale bar = 50 μm. B. Quantification of TUNEL-positive cells (upper), LDH release (middle), and cell viability by CCK-8 assay (lower) in TE10 cells (left) and KYSE70 cells (right) under the indicated conditions (n = 3). The same letter indicates no significant difference between groups, while different letters indicate significant differences between groups. C. Western blot analysis of the indicated proteins in TE10 cells (left, with empty vector, KDM4D-OE, or KDM4D-OE/c-Myc-OE) and KYSE70 cells (right, with sh-Scr, sh-KDM4D, or sh-KDM4D/sh-c-Myc) with or without 4 Gy irradiation.

D. Representative TUNEL staining images in TE10 cells (upper panels: control, KDM4D-OE, KDM4D-OE/sh-SRBD1) and KYSE70 cells (lower panels: control, sh-KDM4D, sh-KDM4D/SRBD1-OE) with or without 4 Gy irradiation. Scale bar = 50 μm. E. Quantification of TUNEL-positive cells (upper), LDH release (middle), and cell viability by CCK-8 assay (lower) in TE10 cells (left) and KYSE70 cells (right) under the indicated conditions (n = 3). The same letter indicates no significant difference between groups, while different letters indicate significant differences between groups. F. Western blot analysis of the indicated proteins in TE10 cells (left, with empty vector, KDM4D-OE, or KDM4D-OE/sh-SRBD1) and KYSE70 cells (right, with sh-Scr, sh-KDM4D, or sh-KDM4D/SRBD1-OE) with or without 4 Gy irradiation.

Discussion

Radiotherapy remains a cornerstone int the treatment of locally advanced ESCC; however, radioresistance remains a major clinical challenge [3]. This study verified KDM4D as a previously unrecognized regulator of ESCC radiosensitivity and delineated the corresponding downstream signaling pathways. Our findings demonstrate that elevated KDM4D expression predicts a favorable response to neoadjuvant chemoradiotherapy, which is mechanistically mediated through activation of the SRBD1/RPL11/c-Myc/WIP1/CHK1 signaling axis.

Our bioinformatics analysis revealed that KDM4D is overexpressed in ESCC tissues compared to normal esophageal mucosa. Notably, high KDM4D expression was associated with better overall survival. This seemingly contradictory finding is consistent with our clinical observation that patients with high KDM4D expression exhibited enhanced sensitivity to neoadjuvant radiotherapy. These data suggest that while KDM4D may contribute to ESCC development, it may also function as a radiosensitizer. This dual role is consistent with the concept of “oncogene addiction”, where cancer cells become dependent on specific oncogenic pathways that can be therapeutically exploited [22].

We identified SRBD1 as a key downstream effector of KDM4D. Analysis of ChIP-seq data revealed an H3K9me3-enriched region within intron 1 of SRBD1 (chr2: 45,610,800-45,611,200 bp). Luciferase reporter assays demonstrated that overexpressing KDM4D significantly enhanced SRBD1 promoter activity, whereas this effect was abrogated upon deletion of the H3K9me3 site (chr2: 45,610,900-45,611,100 bp). Consistent with its role as a histone demethylase, KDM4D overexpression reduced H3K9me3 levels at the SRBD1 intronic region, thereby relieving transcriptional repression and promoting SRBD1 expression. Collectively, these data indicate that KDM4D activates SRBD1 transcription through H3K9-me3 demethylation at a specific intronic regulatory region, which in turn regulates downstream signaling pathways associated with radiosensitivity [23].

The connection between SRBD1 and RPL11 represents a novel regulatory mechanism that links epigenetic regulation to ribosomal protein -mediated tumor suppression. RPL11 has been extensively characterized as a tumor suppressor that inhibits c-Myc activity through multiple mechanisms, including protein-protein interaction and promotion of c-Myc mRNA degradation through the RNA-induced silencing complex (RISC) [14]. Previous studies have demonstrated that SRBD1 regulates RPL11 expression and exerts tumor-suppressive effects in glioma [16], while the RPL11/c-Myc axis has been implicated in modulating chemotherapy sensitivity in breast cancer [24]. Our data demonstrate that KDM4D upregulates RPL11 in a SRBD1-dependent manner, thereby suppressing c-Myc and its downstream targets WIP1 and CHK1. This pathway provides a mechanistic explanation for the radiosensitizing effect associated with high KDM4D expression. Of note, as an S1 RNA-binding domain-containing protein, SRBD1 is likely to regulate RPL11 expression at the post-transcriptional level, potentially through interaction with RPL11 mRNA and modulation of its stability or translational efficiency. This is consistent with the known function of S1 domain proteins, which typically interact with RNA targets. Although direct binding between SRBD1 and RPL11 mRNA was not assessed through RIP assays using anti-SRBD1 antibody, our observation that KDM4D manipulation altered RPL11 expression at both the mRNA and protein levels in a SRBD1-dependent manner provides indirect support for this regulatory relationship. The precise molecular mechanism by which SRBD1 regulates RPL11 warrants further investigation.

The c-Myc-CHK1 axis plays a central role in mediating radioresistance. Previous studies have established that c-Myc transcriptionally

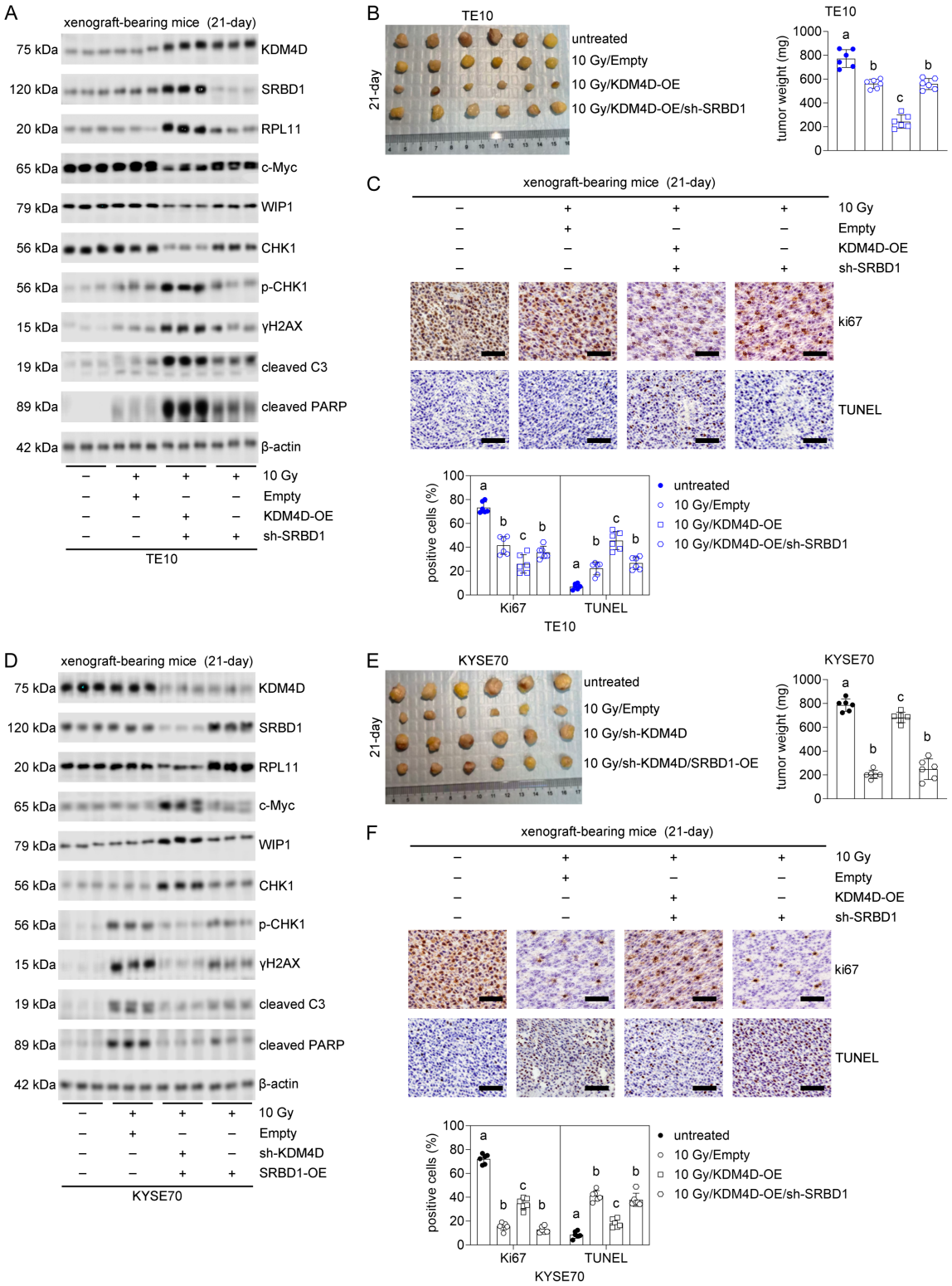

Figure 7. In vivo validation of the KDM4D-SRBD1 axis in regulating ESCC radiosensitivity using xenograft models. A. Western blot analysis of the indicated proteins in xenograft tumor tissues from TE10 cells with empty vector, KDM4D-OE, or KDM4D-OE/sh-SRBD1, with or without 10 Gy irradiation (n = 3 per group). B. Upper: Representative images of xenograft tumors from TE10 cells at day 21 post-irradiation. Lower: Quantification of tumor weights from untreated, 10 Gy/empty vector, 10 Gy/KDM4D-OE, and 10 Gy/KDM4D-OE/sh-SRBD1 groups (n = 6 per group). The same letter indicates no significant difference between groups, while different letters indicate significant dif-

ferences between groups. C. Representative immunohistochemical staining of Ki67 (upper) and TUNEL staining (lower) in xenograft tumor sections from TE10 cells under the indicated conditions. Scale bar = 200 μm. Lower panel, Quantification of Ki67-positive cells (left) and TUNEL-positive cells (right) from at least five random high-power fields per section in untreated, 10 Gy/empty vector, 10 Gy/KDM4D-OE and 10 Gy/KDM4D-OE/sh-SRBD1 groups (n = 6 per group). Different letters indicate significant differences. D. Western blot analysis of the indicated proteins in xenograft tumor tissues from KYSE70 cells with empty vector, sh-KDM4D, or sh-KDM4D/SRBD1-OE, with or without 10 Gy irradiation (n = 3 per group). E. Upper: Representative images of xenograft tumors from KYSE70 cells at day 21 post-irradiation. Lower: Quantification of tumor weights from untreated, 10 Gy/empty vector, 10 Gy/sh-KDM4D, and 10 Gy/sh-KDM4D/SRBD1-OE groups (n = 6 per group).The same letter indicates no significant difference between groups, while different letters indicate significant differences between groups. F. Representative immunohistochemical staining of Ki67 (upper) and TUNEL staining (lower) in xenograft tumor sections from KYSE70 cells under the indicated conditions. Scale bar = 200 μm. Lower panel, Quantification of Ki67-positive cells (left) and TUNEL-positive cells (right) from at least five random high-power fields per section in untreated, 10 Gy/empty vector, 10 Gy/sh-KDM4D and 10 Gy/sh-KDM4D/SRBD1-OE groups (n = 6 per group). The same letter indicates no significant difference between groups, while different letters indicate significant differences between groups. ESCC, esophageal squamous cell carcinoma.

activates CHK1 via direct binding to E-box motifs within the CHK1 promoter, thereby facilitating DNA damage repair and checkpoint activation [25]. Furthermore, c-Myc has been shown to upregulate WIP1 transcriptionally through E-box elements within the WIP1 promoter region [26, 27]. WIP1 in turn dephosphorylates CHK1 at Ser345, thereby terminating the checkpoint response. In KDM4D-high cells, suppression of c-Myc by the SRBD1/RPL11 axis leads to reduced levels of WIP1 and CHK1, thereby resulting in sustained activation of p-CHK1 after irradiation. This persistent checkpoint activation prevents premature cell cycle re-entry and facilitates apoptosis in cells harboring unrepaired DNA damage.

Interestingly, we observed that SRBD1 expression remained largely unchanged in KYSE70 cells regardless of KDM4D manipulation or radiation treatment. Given that KYSE70 cells harbor a TP53 mutation [17], this finding supports the notion that KDM4D-mediated radiosensitization functions in a p53-independent manner. While the RPL11-MDM2-p53 pathway has been well-characterized [28], our data suggest that RPL11 can suppress c-Myc independently of p53 status, extending the therapeutic applicability of this pathway to p53-mutant tumors, which constitute a significant proportion of ESCC cases.

Our findings carry profound clinical relevance. KDM4D expression may serve as a predictive biomarker for radiotherapy responsiveness in individuals with ESCC. In our cohort of 32 ESCC patients receiving neoadjuvant chemoradiotherapy, patients with high KDM4D expression exhibited a prominently higher favorable response rate (66.7% vs. 21.7%) and extended PFS compared with those with low KDM4D expression. From a therapeutic perspective, targeting the c-Myc/WIP1/CHK1 signaling axis may represent a rational strategy to enhance radiosensitivity in KDM4D-low tumors. The emerging progress in KDM4 inhibitors and c-Myc-targeted therapeutic approaches provides novel prospects for the development of combined therapeutic strategies [29, 30]. Specifically, our findings suggest that in ESCC patients with low KDM4D expression and radiotherapy resistance, the elevated c-Myc activity leads to upregulation of WIP1 and CHK1, promoting premature cell cycle re-entry and dampening the DNA damage checkpoint response. In such cases, pharmacologic inhibition of CHK1, using agents such as UCN-01 or MK-8776, both of which have entered early-phase clinical evaluation and demonstrated radiosensitizing effects in preclinical studies [31], may enhance radiosensitivity by preventing checkpoint recovery and inducing mitotic catastrophe. Alternatively, inhibition of WIP1, such as using GSK2830371, may represent another therapeutic option in tumors retaining wild-type p53 [27, 32], given the critical role of WIP1-mediated dephosphorylation of CHK1 in terminating checkpoint signaling in KDM4D-low tumors. Furthermore, emerging KDM4 family inhibitors, such as the pan-KDM4 inhibitor TACH101 (zavondemstat), which has recently completed a Phase I clinical trial with a favorable safety profile [12, 33], may offer a novel approach to modulate the SRBD1/RPL11/c-Myc axis. Collectively, these findings provide a strong rationale for the development of combination therapeutic strategies targeting this signaling network. Future preclinical and clinical

studies are needed to evaluate the efficacy and safety of these combination strategies.

Several limitations of this study should be acknowledged. First, the clinical sample size of 32 patients is relatively small, with only 9 cases in the high KDM4D expression subgroup, which may have limited statistical power. Although our clinical findings are corroborated by TCGA database analysis and comprehensive *in vitro* and *in vivo* experiments, larger multicenter prospective studies are warranted to validate the predictive value of KDM4D expression. Second, although we established a regulatory relationship between SRBD1 and RPL11, the detailed biochemical mechanisms remain to be elucidated, especially whether SRBD1 directly binds to RPL11 mRNA to regulate its stability or translational efficiency. Third, the therapeutic potential of targeting the c-Myc/WIP1/CHK1 axis in combination with radiotherapy warrants further evaluation in preclinical and clinical settings, particularly in patients with low KDM4D expression.

Conclusion

We identified a novel KDM4D/SRBD1/RPL11/c-Myc/WIP1/CHK1 signaling axis that regulates radiosensitivity in ESCC. Elevated KDM4D expression activates this signaling cascade, leading to suppression of c-Myc activity, downregulation of WIP1 and CHK1, sustained activation of phosphorylated CHK1, and enhanced radiation-induced apoptosis. These findings provide new insight into the molecular basis of radiosensitivity in ESCC and highlight KDM4D as a promising predictive biomarker and potential therapeutic target for optimizing radiotherapy outcome.

Disclosure of conflict of interest

None.

Address correspondence to: Dr. Shuanghu Yuan, Department of Radiation Oncology, Shandong University Cancer Center, 440 Jiyan Road, Huaiyin District, Jinan 250012, Shandong, China. E-mail: yuanshuanghu0216@126.com

References

[1] Morgan E, Soerjomataram I, Rumgay H, Coleman HG, Thrift AP, Vignat J, Laversanne M, Ferlay J and Arnold M. The global landscape of esophageal squamous cell carcinoma and esophageal adenocarcinoma incidence and mortality in 2020 and projections to 2040: new estimates from GLOBOCAN 2020. Gastroenterology 2022; 163: 649-658.e642.

[2] Sheikh M, Roshandel G, McCormack V and Malekzadeh R. Current status and future prospects for esophageal cancer. Cancers (Basel) 2023; 15: 765.

[3] Okumura H, Uchikado Y, Setoyama T, Matsumoto M, Owaki T, Ishigami S and Natsugoe S. Biomarkers for predicting the response of esophageal squamous cell carcinoma to neoadjuvant chemoradiation therapy. Surg Today 2014; 44: 421-428.

[4] Katagiri T, Ohyama Y, Miyamoto H, Egawa Y, Moriki T and Hasegawa K. Pathological responses to low-dose irradiation and pepleomycin in oral squamous cell carcinoma are predictive of Locoregional control. BMC Cancer 2020; 20: 1216.

[5] Wang X, Gu M, Ju Y and Zhou J. Overcoming radio-resistance in esophageal squamous cell carcinoma via hypermethylation of PIK3C3 promoter region mediated by KDM5B loss. J Radiat Res 2022; 63: 331-341.

[6] Wang WJ, Wu SP, Liu JB, Shi YS, Huang X, Zhang QB and Yao KT. MYC regulation of CHK1 and CHK2 promotes radioresistance in a stem cell-like population of nasopharyngeal carcinoma cells. Cancer Res 2013; 73: 1219-1231.

[7] Lu X, Nannenga B and Donehower LA. PPM1D dephosphorylates Chk1 and p53 and abrogates cell cycle checkpoints. Genes Dev 2005; 19: 1162-1174.

[8] Manni W, Jianxin X, Weiqi H, Siyuan C and Huashan S. JMJD family proteins in cancer and inflammation. Signal Transduct Target Ther 2022; 7: 304.

[9] Lee DH, Kim GW, Jeon YH, Yoo J, Lee SW and Kwon SH. Advances in histone demethylase KDM4 as cancer therapeutic targets. FASEB J 2020; 34: 3461-3484.

[10] Khoury-Haddad H, Guttmann-Raviv N, Ipenberg I, Huggins D, Jeyasekharan AD and Ayoub N. PARP1-dependent recruitment of KDM4D histone demethylase to DNA damage sites promotes double-strand break repair. Proc Natl Acad Sci U S A 2014; 111: E728-737.

[11] Bur H, Haapasaari KM, Turpeenniemi-Hujanen T, Kuittinen O, Auvinen P, Marin K, Soini Y and Karihtala P. Strong KDM4B and KDM4D expression associates with radioresistance and aggressive phenotype in classical Hodgkin lymphoma. Anticancer Res 2016; 36: 4677-4683.

[12] Chandhasin C, Dang V, Perabo F, Del Rosario J, Chen YK, Filvaroff E, Stafford JA and Clarke M. TACH101, a first-in-class pan-inhibitor of KDM4 histone demethylase. Anticancer Drugs 2023; 34: 1122-1131.

[13] Dai MS, Sears R and Lu H. Feedback regulation of c-Myc by ribosomal protein L11. Cell Cycle 2007; 6: 2735-2741.
[14] Khongkow P, Karunarathna U, Khongkow M, Gong C, Gomes AR, Yagüe E, Monteiro LJ, Kongsema M, Zona S, Man EP, Tsang JW, Coombes RC, Wu KJ, Khoo US, Medema RH, Freire R and Lam EW. FOXM1 targets NBS1 to regulate DNA damage-induced senescence and epirubicin resistance. Oncogene 2014; 33: 4144-4155.
[15] Writing Committee for the Normal Tension Glaucoma Genetic Study Group of Japan Glaucoma Society, Meguro A, Inoko H, Ota M, Mizuki N and Bahram S. Genome-wide association study of normal tension glaucoma: common variants in SRBD1 and ELOVL5 contribute to disease susceptibility. Ophthalmology 2010; 117: 1331-1338.e5.
[16] Chen H, Gao S, Wang P, Xie M, Zhang H, Fan Y, Nie E and Lan Q. SRBD1 regulates the cell cycle, apoptosis, and M2 macrophage polarization via the RPL11-MDM2-p53 pathway in glioma. Environ Toxicol 2025; 40: 66-78.
[17] Ji J, Wu K, Wu M and Zhan Q. p53 functional activation is independent of its genotype in five esophageal squamous cell carcinoma cell lines. Front Med China 2010; 4: 412-418.
[18] Stewart-Ornstein J, Iwamoto Y, Miller MA, Prytyskach MA, Ferretti S, Holzer P, Kallen J, Furet P, Jambhekar A, Forrester WC, Weissleder R and Lahav G. p53 dynamics vary between tissues and are linked with radiation sensitivity. Nat Commun 2021; 12: 898.
[19] Wei H, Wang H, Wang G, Qu L, Jiang L, Dai S, Chen X, Zhang Y, Chen Z, Li Y, Guo M and Chen Y. Structures of p53/BCL-2 complex suggest a mechanism for p53 to antagonize BCL-2 activity. Nat Commun 2023; 14: 4300.
[20] O'Geen H, Bates SL, Carter SS, Nisson KA, Halmai J, Fink KD, Rhie SK, Farnham PJ and Segal DJ. Ezh2-dCas9 and KRAB-dCas9 enable engineering of epigenetic memory in a context-dependent manner. Epigenetics Chromatin 2019; 12: 26.
[21] Han Q, Zhou Y, Dong Z, Wang W, Wang M, Pang M, Song X, Chen B and Zheng A. SNORA47 affects stemness and chemotherapy sensitivity via EBF3/RPL11/c-Myc axis in luminal A breast cancer. Mol Med 2025; 31: 150.
[22] Kang J, Brajanovski N, Chan KT, Xuan J, Pearson RB and Sanij E. Ribosomal proteins and human diseases: molecular mechanisms and targeted therapy. Signal Transduct Target Ther 2021; 6: 323.
[23] Zhu Y, van Essen D and Saccani S. Cell-type-specific control of enhancer activity by H3K9 trimethylation. Mol Cell 2012; 46: 408-423.
[24] Han Q, Zhou Y, Dong Z, Wang W, Wang M, Pang M, Song X, Chen B and Zheng A. Correction: SNORA47 affects stemness and chemotherapy sensitivity via EBF3/RPL11/c-Myc axis in luminal A breast cancer. Mol Med 2025; 31: 220.
[25] Mak JP, Man WY, Chow JP, Ma HT and Poon RY. Pharmacological inactivation of CHK1 and WEE1 induces mitotic catastrophe in nasopharyngeal carcinoma cells. Oncotarget 2015; 6: 21074-21084.
[26] Eren MK, Kartal NB and Pilevneli H. Oncogenic WIP1 phosphatase attenuates the DNA damage response and sensitizes p53 mutant Jurkat cells to apoptosis. Oncol Lett 2021; 21: 479.
[27] Pechackova S, Burdova K, Benada J, Kleiblova P, Jenikova G and Macurek L. Inhibition of WIP1 phosphatase sensitizes breast cancer cells to genotoxic stress and to MDM2 antagonist nutlin-3. Oncotarget 2016; 7: 14458-14475.
[28] Temaj G, Saha S, Dragusha S, Ejupi V, Buttari B, Profumo E, Beqa L and Saso L. Ribosomopathies and cancer: pharmacological implications. Expert Rev Clin Pharmacol 2022; 15: 729-746.
[29] Ni F, Tang H, Cheng S, Yu Y, Yuan Z, Chen Y, Zhang E and Wang X. KDM4B: a promising oncology therapeutic target. Cancer Sci 2024; 115: 8-16.
[30] Duffy MJ, O'Grady S, Tang M and Crown J. MYC as a target for cancer treatment. Cancer Treat Rev 2021; 94: 102154.
[31] Suzuki M, Yamamori T, Bo T, Sakai Y and Inanami O. MK-8776, a novel Chk1 inhibitor, exhibits an improved radiosensitizing effect compared to UCN-01 by exacerbating radiation-induced aberrant mitosis. Transl Oncol 2017; 10: 491-500.
[32] Gilmartin AG, Faitg TH, Richter M, Groy A, Seefeld MA, Darcy MG, Peng X, Federowicz K, Yang J, Zhang SY, Minthorn E, Jaworski JP, Schaber M, Martens S, McNulty DE, Sinnamon RH, Zhang H, Kirkpatrick RB, Nevins N, Cui G, Pietrak B, Diaz E, Jones A, Brandt M, Schwartz B, Heerding DA and Kumar R. Allosteric Wip1 phosphatase inhibition through flap-subdomain interaction. Nat Chem Biol 2014; 10: 181-187.
[33] Tsimberidou AM, Dayyani F, Sommerhalder D, Vandross AL, Pelster MS, Henry JT, Perez CA, Chakraborty A, Baysal MA, Chandhasin C, Dai Y, Tu S, King I and Perabo F. Phase 1 study of zavondemstat (TACH101), a first-in-class KDM4 inhibitor, in patients with advanced solid tumors. Oncologist 2025; 30: oyaf169.

Supplementary Table 1. Primer sequences used for RT-qPCR analysis

Species	Gene	Forward Primer (5'-3')	Reverse Primer (5'-3')
Human	KDM4D	GGGCAGGGGTGTTTACTCAAT	TGTTTGCCAAATGGCGATACT
Human	WIP1	GCCAGAACTTCCCAAGGAAAG	GGTTCAGGTGACACCACAAATTC
Human	RPL11	AGAGTGGAGACAGACTGACGCG	CGGATGCCAAAGGATCTGACAG
Human	CHK1	GTGTCAGAGTCTCCCAGTGGAT	GTTCTGGCTGAGAACTGGAGTAC
Human	SRBD1	CCTTCCAACAGTGTGCTGGCTT	GTGACCTCAACGTCTGCTGAAG
Human	c-Myc	CCTGGTGCTCCATGAGGAGAC	CAGACTCTGACCTTTTGCCAGG
Human	β-actin	CACCATTGGCAATGAGCGGTTC	AGGTCTTTGCGGATGTCCACGT

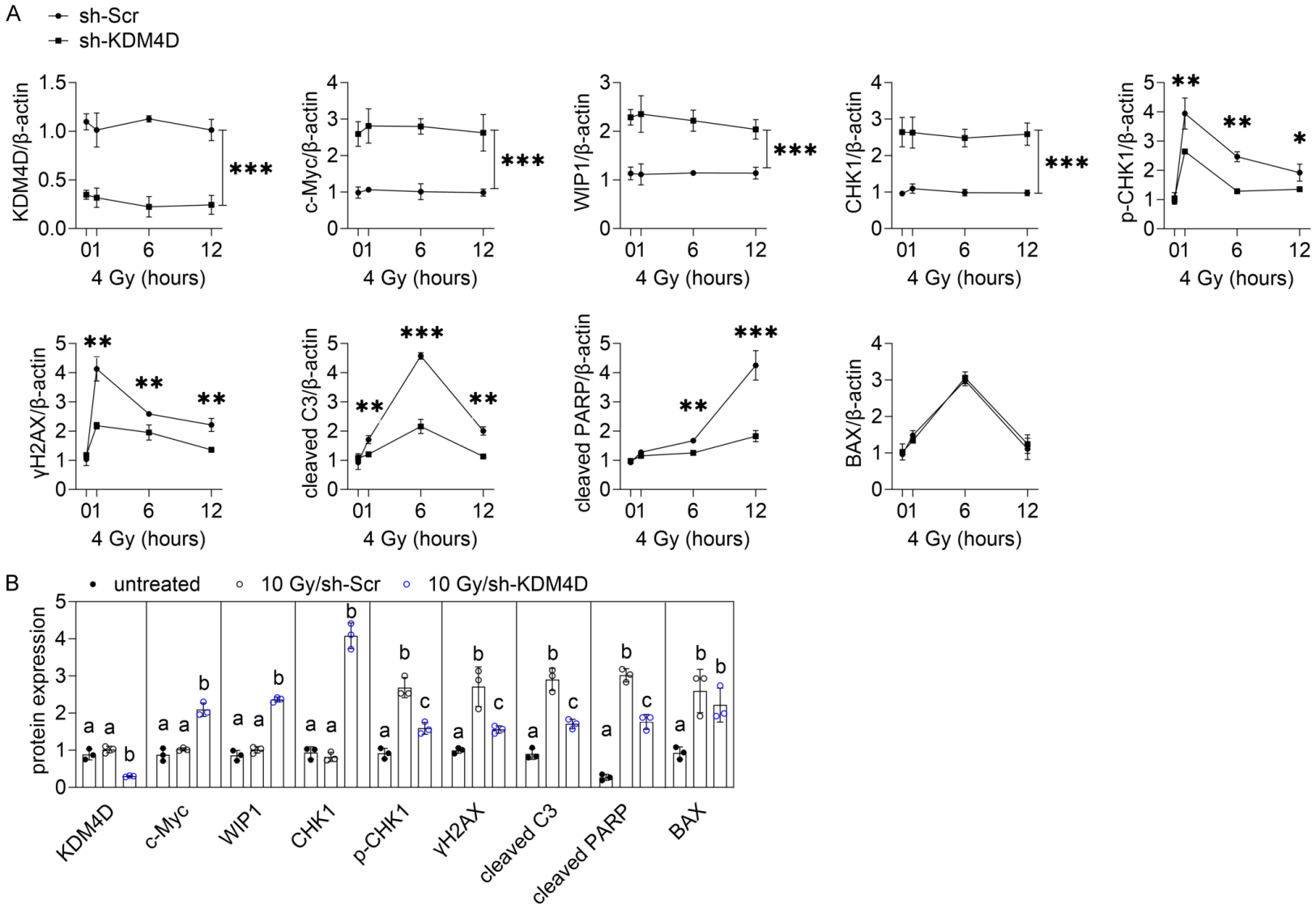

Supplementary Figure 1. Quantification of western blot data from **Figure 3E** and **3G**. A. Quantification of protein expression levels (normalized to β-actin) from western blots in **Figure 3E**, showing KDM4D, c-Myc, WIP1, CHK1, p-CHK1, γH2AX, cleaved caspase-3, cleaved PARP and BAX in KYSE70 cells with sh-Scr or sh-KDM4D at indicated time points after 4 Gy irradiation (n = 3). *$P < 0.05$, **$P < 0.01$, ***$P < 0.001$. B. Quantification of protein expression levels from western blots in **Figure 3G**, showing the indicated proteins in xenograft tumor tissues from untreated, 10 Gy/sh-Scr and 10 Gy/sh-KDM4D groups (n = 3). Different letters indicate significant differences.

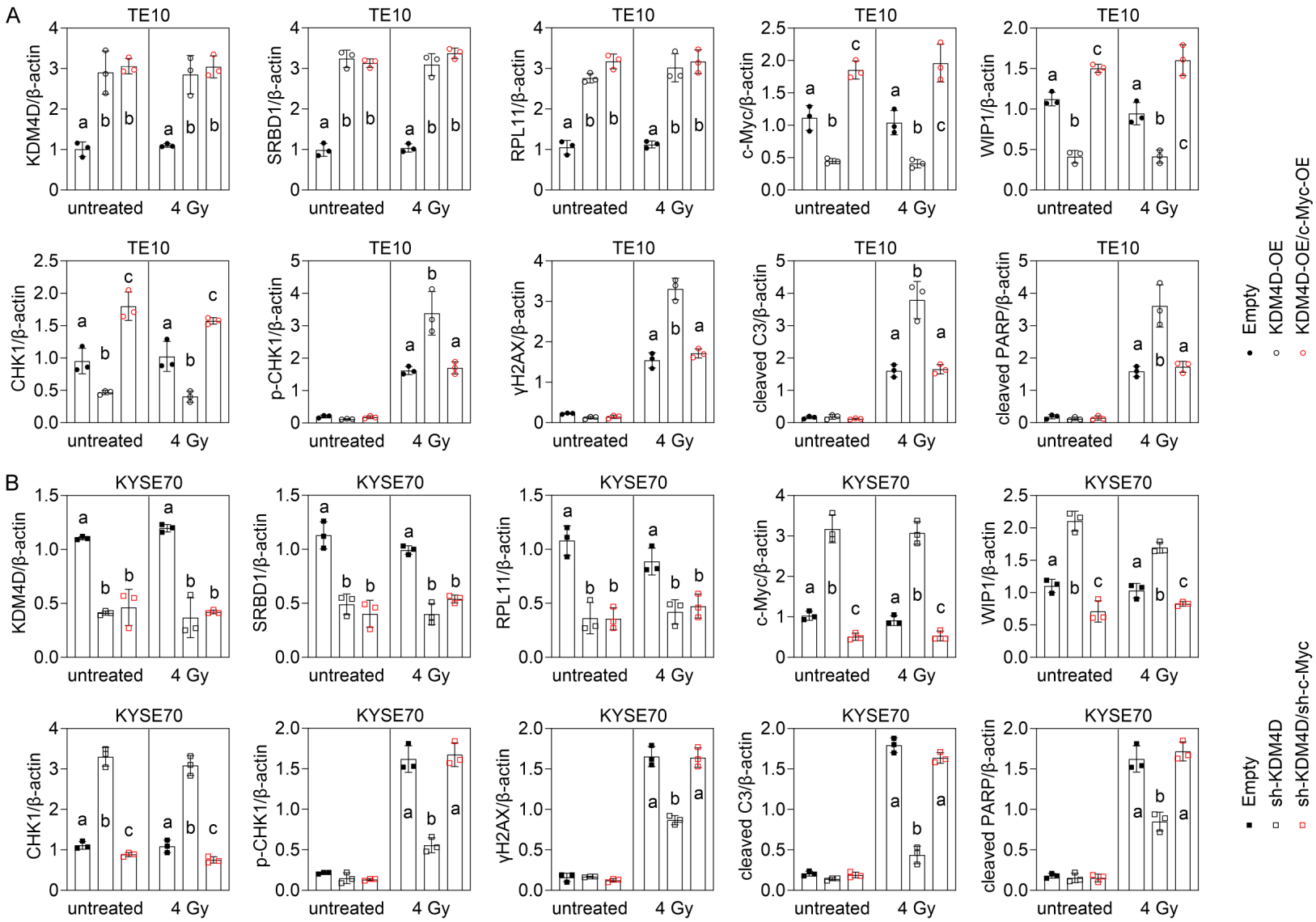

Supplementary Figure 2. Quantification of western blot data from **Figure 6C**. A. Quantification of protein expression levels in TE10 cells with empty vector, KDM4D-OE, or KDM4D-OE/c-Myc-OE, with or without 4 Gy irradiation (n = 3). Different letters indicate significant differences. B. Quantification of protein expression levels in KYSE70 cells with sh-Scr, sh-KDM4D, or sh-KDM4D/sh-c-Myc, with or without 4 Gy irradiation (n = 3). The same letter indicates no significant difference between groups, while different letters indicate significant differences between groups.

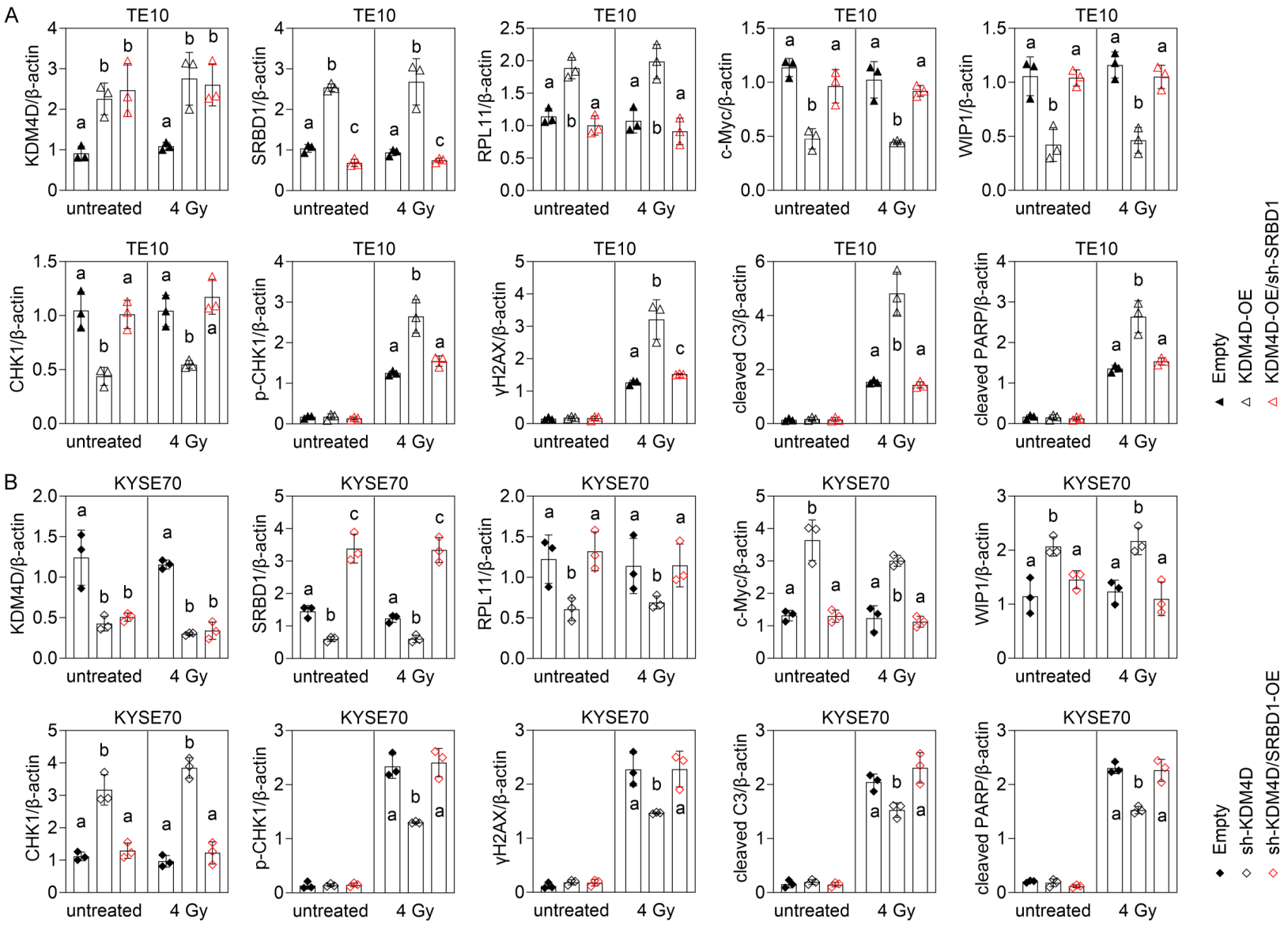

Supplementary Figure 3. Quantification of western blot data from **Figure 6F**. A. Quantification of protein expression levels in TE10 cells with empty vector, KDM4D-OE, or KDM4D-OE/sh-SRBD1, with or without 4 Gy irradiation (n = 3). Different letters indicate significant differences. B. Quantification of protein expression levels in KYSE70 cells with sh-Scr, sh-KDM4D, or sh-KDM4D/SRBD1-OE, with or without 4 Gy irradiation (n = 3). The same letter indicates no significant difference between groups, while different letters indicate significant differences between groups.

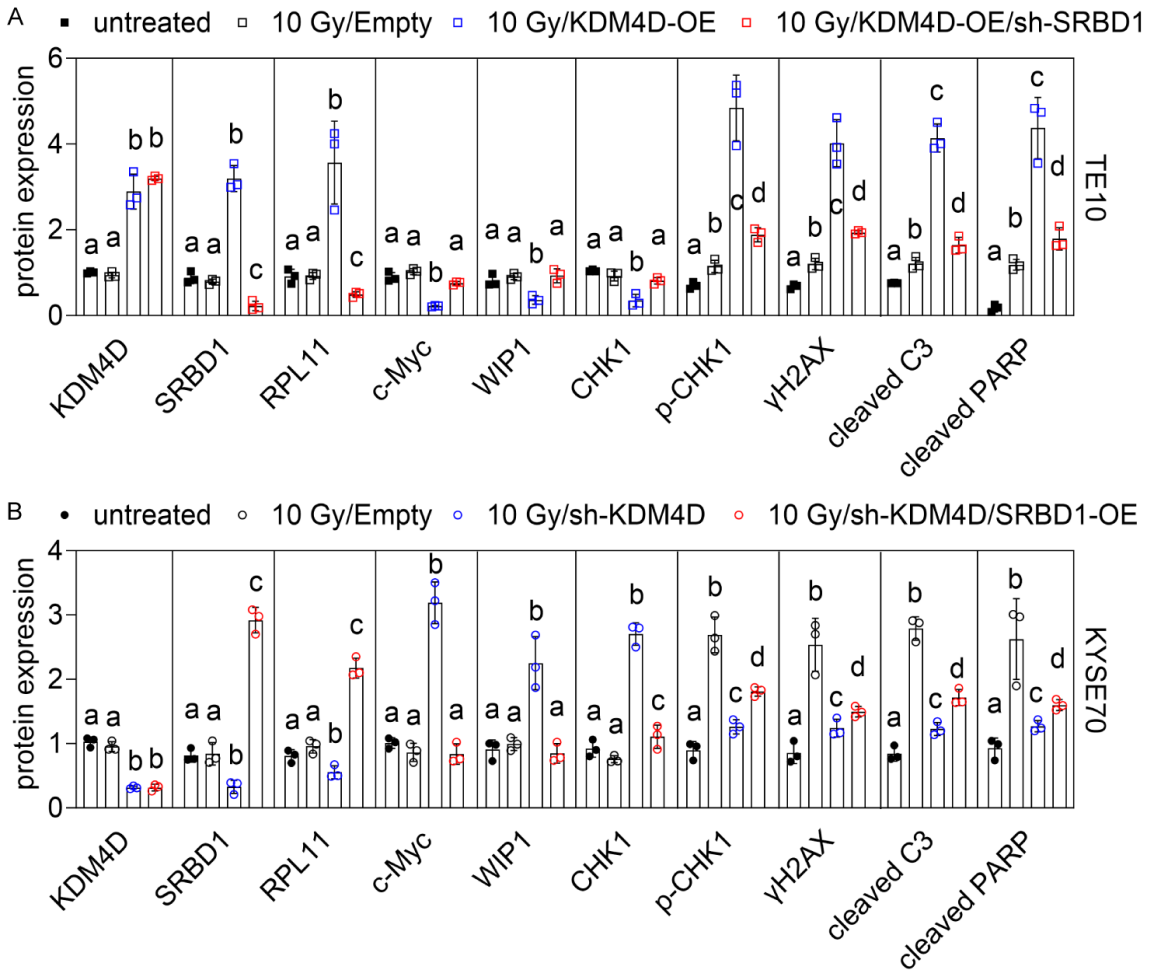

Supplementary Figure 4. Quantification of western blot data from **Figure 7A** and **7D**. A. Quantification of protein expression levels in xenograft tumor tissues from TE10 cells under the indicated conditions (n = 3). Different letters indicate significant differences. B. Quantification of protein expression levels in xenograft tumor tissues from KYSE70 cells under the indicated conditions (n = 3). The same letter indicates no significant difference between groups, while different letters indicate significant differences between groups.